A lateralized pathway for associating nutrients with flavors

James C. R. Grove[1,2,3,4], Anna M. Hakimi[1,2,3], Queenie Li[4], Jingkun Zhang[4], Heiko Backes[5], Bojana Kuzmanovic[5], Jaewon Choi[4], Violeta Ubadiah[4], Longhui Qiu[6], Zhengya Liu[1,2,3], Dana M. Small[7,8], Marc Tittgemeyer[5], Zachary A. Knight[1,2,3,4,9*].

[1]Department of Physiology, University of California, San Francisco
[2]Kavli Institute for Fundamental Neuroscience, University of California, San Francisco
[3]Neuroscience Graduate Program, University of California, San Francisco
[4]Howard Hughes Medical Institute
[5]Max Planck Institute for Metabolism Research, Cologne, Germany
[6]Department of Medicine, University of California, San Francisco
[7]Department of Psychiatry, Yale University School of Medicine
[8]Department of Psychology, Yale University School of Medicine
[9]Weill Institute for Neurosciences, University of California, San Francisco

[*] Corresponding author: zachary.knight@ucsf.edu

Abstract

Animals learn about the external world, in part, via interoceptive signals[1,2]. For example, the nutrient content of food is first estimated in the mouth, in the form of flavor, and then measured again via slower signals from the gut. How these signals from the mouth and gut are integrated to drive learning is unknown. Here we identify a lateralized dopamine pathway that is specialized for learning about the nutrient content of food. We show that dopamine neurons in the ventral tegmental area (VTA_{DA}) are necessary for associating nutrients with flavors, and that post-ingestive nutrients trigger DA release selectively in a small region of the anterior basolateral amygdala (BLA) but not canonical DA targets in striatum. Remarkably, this nutrient-triggered DA release occurs preferentially on the left side of the brain in both mice and humans, revealing that the DA system is functionally lateralized. We identify the gut sensors that are responsible for nutrient-triggered DA release; show that they activate BLA-projecting DA neurons defined by expression of cholecystokinin (CCK); and demonstrate that stimulation of DA axon terminals in the anterior BLA drives flavor-nutrient learning but not other aspects of feeding behavior. Two-photon imaging of neurons in the left anterior BLA reveals that they integrate gustatory and post-ingestive cues, and silencing these neurons prevents flavor-nutrient learning. These findings establish a neural basis for how animals learn about the

35 nutrient content of their food. They also reveal unexpectedly that post-ingestive nutrients are differentially represented on the right and left sides of the brain.

Introduction

We learn about food during the process of eating[1–4]. For example, animals come to prefer calorie-rich foods after experiencing their post-ingestive effects[1,2]. This learning process is
40 enabled by sensation along the alimentary canal that begins at the tip of the tongue and extends into the intestine. A fundamental challenge is to explain how these diverse interoceptive signals are integrated in the brain to create a coherent picture of what has been consumed.

Prior work has shown that there is a privileged connection between sensory signals that arise from the mouth and gut. For example, animals can learn to lick a flavored solution, but not press
45 a lever, in order to receive an infusion of nutrients into the stomach[5,6]. This suggests that there may be hardwired pathways in the brain for linking orosensory and gut signals, but the identity and nature of these circuits is unknown.

DA neurons are required for learning about nutrients but not toxins

We first tested whether VTA_{DA} neurons are required for learning associations between nutrients
50 and flavors[7–9]. We targeted the inhibitory opsin stGtACR to these cells for neural silencing, and, in a separate surgery, equipped mice with intragastric (IG) catheters for nutrient infusion. We then used a closed-loop paradigm for post-ingestive learning[5,10] in which mice are given access to two differentially flavored solutions, one of which is paired with lick-triggered IG glucose infusion and the other of which is paired with isovolumic infusions of water (see Methods, Fig.
55 1a). After six days of training, the preference of mice for these two flavors is measured in a two-bottle test. Consistent with previous findings[10], we found that control mice developed a robust preference for the solution paired with sugar infusion (35±5% before vs. 81±7% after training, p=7.8e-5). In contrast, optogenetic silencing of VTA_{DA} neurons throughout training completely blocked the acquisition of a flavor preference (48±7% before vs. 53±7% after training, Fig. 1b;
60 Extended Fig. 1). Importantly, silencing VTA_{DA} neurons did not reduce consumption of foods with known caloric value (Fig. 1d). However, it did reduce the consumption of food with a larger than expected caloric content (i.e. on the first day that a flavor was paired with closed-loop nutrient infusion; Fig. 1c). This suggests that VTA_{DA} neurons are necessary for updating food preferences and consumption in response to new information about a food's caloric content.

65 In addition to learning to prefer foods that have calories, animals also learn to avoid foods that are toxic, which occurs through an analogous post-ingestive learning process known

as conditioned flavor avoidance[11–13] (CFA). To test whether VTA_{DA} neurons are involved in learning about toxins, we asked whether silencing these cells could block the CFA that results from pairing a novel flavor with LiCl injection, which causes visceral malaise (Fig. 1e). In contrast to flavor-nutrient learning (Fig. 1b), we found that silencing VTA neurons had no effect on flavor-toxin learning (Fig. 1e). This indicates that VTA_{DA} neurons are specifically required for learning about nutrients but are not necessary for all forms of post-ingestive learning.

Nutrients selectively trigger DA release in the BLA

We hypothesized that DA neurons contribute to flavor nutrient conditioning by supplying a signal of nutrient detection from the gut. Of note, previous studies have reported post-ingestive DA release in multiple brain regions[14–19], but the significance of these pathways for post-ingestive learning has not been tested.

We first directly compared nutrient-triggered DA release in three principal targets of VTA_{DA} neurons: the nucleus accumbens core (NAc), dorsolateral striatum (DLS), and two sites in the basolateral amygdala (medial, mBLA; and lateral, latBLA). We targeted GRAB-DA3m[20] to these structures for fiber photometry recordings of extracellular DA and in the same surgery installed IG catheters for nutrient infusion (Fig. 2a; Extended Figs. 2, 3). Infusion of the complete diet Ensure caused dramatic DA release in mBLA (18.2±3.5%, p=1e-5) which began 48±11 seconds after nutrients entered the stomach, and remained elevated for 9±1 minutes after the infusion ended (Extended Fig. 3a–i). This response was specific to nutrients, as it was also observed for infusion of glucose but not water (13.5±4.0% vs. -0.1±0.3% p=3e-5) or mannitol (Extended Fig. 3d), and it was independent of sex, as it was observed in both male and female mice (Extended Fig. 3c). In contrast, less nutrient-triggered DA release was observed in latBLA and none in dorsal or ventral striatum (Fig. 2a; Extended Fig. 3j–q). This is consistent with our prior finding that nutrient detection in the gut does not trigger DA release in the other major targets of the mesolimbic DA pathway[14].

To confirm that these DA dynamics in BLA also occur during natural ingestion, we next recorded DA release during self-paced consumption of Ensure (Fig. 2b; Extended Fig. 4). In mBLA, we observed a dramatic increase in DA release that ramped during the first minute of ingestion and was sustained for the entire trial (Fig. 2b–d; Extended Fig. 4a–e). In contrast, DA release in NAc peaked almost immediately after ingestion and then rapidly declined, consistent with known responses in NAc to appetitive tastes (Extended Fig. 4j–m). Interestingly, we observed a small but statistically significant (1.0±0.3%, p=1e-4; Extended Fig. 4q) increase in DA release in DLS after ingestion that may correspond to previous observations using microdialysis[16–19]. Together,

100 this indicates that the mBLA is the major site of DA release in response to nutrient detection in the gut.

DA release in response to nutrients is restricted to the anterior BLA

The BLA is an extended structure that spans 2.5 mm in the rostro-caudal axis in the mouse,
105 and its anterior and posterior subdivisions have differences in cytoarchitecture, connectivity, and food cue responses[21–24]. Of note, the mBLA, where we observed the largest DA responses, is part of the magnocellular region that extends to anterior BLA, whereas the latBLA is part of the parvocellular region that extends posteriorly (Extended Fig. 3n). We therefore prepared mice for DA recordings in anterior vs. posterior BLA to test directly whether there is differential DA
110 release across the rostro-caudal axis (Fig. 2e; Extended Figs. 5, 6). This revealed that nutrient infusion caused much larger DA release in the anterior versus posterior BLA (e.g. Ensure: 10.0±2.3% vs. 3.1±0.4%, p=8.5e-3; Fig. 2e). Importantly, we found that the DA release in response to licking – which is immediate and does not involve GI signals – was the same in the anterior and posterior BLA, indicating that the difference in GI responses was not due to a
115 technical defect in our posterior BLA recordings (Fig. 2f, Extended Figs. 5a–c; 6a–b). Indeed, we found that DA release in posterior BLA was preferentially triggered by aversive GI stimuli, such as injection of LiCl (Extended Fig. 5g) and LPS (Extended Fig. 5h), which did not cause DA release in anterior BLA. This shows that the anterior and posterior BLA respond to fundamentally different visceral signals.

120 We next investigated the gut sensors that detect nutrients upstream of the BLA. We reasoned that, if this pathway is involved in flavor-nutrient learning, then DA release in the anterior BLA should depend on the specific gut receptors that have been implicated in this process. For sugar, it has been shown that the key sensor is the intestinal sodium glucose transporter SGLT1[25,26]. Consistently, we found that IG infusion of a variety of SGLT1 agonists (glucose,
125 galactose, and MDG) induced strong DA release in anterior BLA, whereas sugars that do not activate SGLT1 (mannitol and fructose) did not stimulate DA release (Extended Fig. 6g). Conversely, blocking intestinal SGLT1 with a specific antagonist was sufficient to prevent anterior BLA DA release in response IG glucose infusion (Extended Fig. 6h), indicating that this transporter is necessary. For fat, the key intestinal sensors are GPR40/120 and CD36[27–29].
130 Accordingly, we found that blocking all three of these intestinal receptors abolished DA release

in the anterior BLA during fat infusion (Extended Fig. 6j). Thus, DA release in the anterior BLA depends on the same gut sensors that are known to drive flavor-nutrient conditioning.

CCK+ DA neurons that project to BLA preferentially respond to nutrients

Our finding that nutrients trigger DA release only in the anterior BLA suggests that these responses are driven by only a small percentage of all VTA_{DA} neurons. Indeed, when we performed single-cell calcium imaging of all VTA_{DA} neurons, we observed that only 11% of cells were activated during IG nutrient infusion[14,30] (Fig. 3a). We therefore set out to identify these nutrient-responsive DA neurons.

Previous anatomic studies have shown that VTA_{DA} neurons expressing cholecystokinin ($VTA_{DA,CCK}$) project preferentially to the BLA[31], whereas VTA_{DA} neurons expressing the leptin receptor ($VTA_{DA,LepR}$) project to the adjacent central amygdala[32] (CeA). We therefore targeted GCaMP7s to these cells using an intersectional genetic approach and performed single-cell imaging in response to nutrient infusions (Fig. 3b; Extended Fig. 7). Consistent with our photometry results, we found that a majority of $VTA_{DA\text{-}CCK}$ cells (61%) were activated during nutrient infusion in manner that mirrored the DA dynamics in the BLA (Fig. 3c). For example, somatic calcium ramped in the first minute after the onset of infusion (rise time: 36±7s for calcium vs. 41±12s for DA in BLA; see Methods; Extended Fig. 3f–g, 7e) and then remained elevated for many minutes after nutrient infusion ended (Extended Fig. 7g).

While most $VTA_{DA\text{-}CCK}$ neurons responded to IG nutrients, these responses were not homogeneous. Indeed, k-means clustering revealed two populations of $VTA_{DA\text{-}CCK}$ cells, one that was activated primarily during IG infusion and a second population of cells that showed more sustained responses (Fig. 3d). Consistently, principal component analysis (PCA) revealed two distinct phases of activity—one during nutrient infusion (PC2) and one after (PC1) (Fig. 3e)—and this first principle component was sufficient to segregate the two clusters of cells identified by k-means (Extended Fig. 7f). This reveals that internal signals of nutrient ingestion – which persist for tens for minutes – are encoded in two parts by two discrete populations of CCK+ DA cells at the level of the VTA.

We found that $VTA_{DA\text{-}LepR}$ neurons also showed strong and sustained responses to IG nutrient infusion (Fig. 3f–h; Extended Fig. 8). Consistent with this, we found that IG nutrients triggered robust DA release in the CeA (Fig. 3i; Extended Fig. 9). We confirmed that this DA release was distinct from the DA release in adjacent BLA by using region-specific Cre drivers (Vgat for CeA, Vglut2 for BLA) to confine GRAB-DA to the respective nuclei. Moreover, we found that the DA

release during natural ingestion peaked much earlier in CeA compared to BLA (3.4±0.7 s vs 21.7±2.3 s, p=4.7e-3 ; Fig. 3j–k; Extended Figs. 9c–d, 9h–i), suggesting that DA release in these two structures may have distinct functions.

The VTA→anterior BLA pathway is specialized for post-ingestive learning

We next investigated which of these DA pathways is involved in learning about nutrients and flavors (Fig. 4a). We prepared mice for optogenetic stimulation of VTA_{DA} terminals in the anterior BLA and CeA, which both show strong nutrient-induced DA release, as well three other control sites: the posterior BLA, which we found responded to aversive visceral signals (Fig. 2,3, Extended Figs. 3–6,9), and the NAc and DLS, which are important for many other forms of DA-mediated learning[33–35].

We reasoned that if nutrient-triggered DA release in a brain region drives flavor learning, then optogenetically-induced DA release in that structure should substitute for IG infusion. Mice were given access to two differently flavored, non-caloric solutions, one of which was paired with stimulation following a 20s delay (to mimic the time course of post-ingestive DA release; see Methods and Extended Data Fig. 3e), while the other solution did not trigger stimulation. Strikingly, this delayed stimulation of DA release in anterior BLA conditioned a robust flavor preference (Fig. 4b; Extended Fig. 10b), whereas no increase preference was observed after stimulation of axon terminals in any other region. This indicates that only the anterior BLA projection is sufficient to drive flavor learning.

To evaluate the specificity of these results, we tested these mice in a battery of assays measuring different aspects of feeding behavior or reinforcement. In contrast to the effects on flavor learning, stimulation of axon terminals in the anterior BLA had no effect on total food intake, regardless of the timing of optogenetic stimulation (either continuous or closed-loop to lick onset or offset; see Methods; Fig. 4e–g; Extended Fig. 10c–e) and also failed to condition avoidance of a paired flavor (Fig. 4c). This pathway also failed to support self-stimulation, indicating it is not reinforcing in the absence of a flavor cue[36] (Fig. 4d). Thus, DA release in anterior BLA influences feeding by specifically driving flavor learning.

Although we saw similar dynamics of nutrient-triggered DA release in CeA, stimulation of the VTA to CeA pathway did not drive flavor learning (Fig. 4b). However, it did potentiate ongoing feeding and drinking behavior, consistent with the idea that DA release in this structure is reinforcing (Fig. 4e–g; Extended Fig. 10c–g). We observed similar effects when stimulating the pathway to NAc[37 35] (Fig. 4e–g; Extended Fig. 10c–g). On the other hand, DA release in DLS

caused a reduction in flavor preference (61.1±6.2% before vs. 36.7%±4.6% after training; p=1.1e-3, Fig. 4b) and there was a trend toward conditioned flavor avoidance (73.9±6.0% vs. 50.0±6.0% sugar preference; p=1.3e-2; Fig. 4c). Taken together, these results reveal a double dissociation in which the anterior BLA pathway drives flavor learning but not other aspects of motivated behavior or reinforcement, which are instead mediated by canonical DA pathways.

Anterior BLA neurons integrate gustatory and post-ingestive signals to drive learning

The fact that nutrients trigger DA release in anterior BLA, and this drives flavor learning, raises the question of how flavors and post-ingestive signals are integrated in this structure. In pilot studies, we found that IG nutrient infusion was unable to condition a preference when it was separated in time from the paired flavor (Extended Fig. 11a), implying that these signals must overlap for learning to occur (which is in contrast to CFA, which permits long delays between flavor and toxin[12]). We therefore prepared mice for two-photon imaging of anterior BLA neurons expressing dopamine receptor 1 (D1R), which labels most DA-responsive BLA cells[38] (Fig. 5a), and examined how these cells integrate ongoing nutrient and flavor signals.

We first sought to isolate BLA responses to flavor cues by recording activity during brief-access taste tests (5 seconds, each trial initiated by an auditory cue) for sucrose, sucralose (a non-caloric sweetener), or water. To distinguish taste-driven activity from other cue responses[24] or licking itself, in 10% of trials (mock trials) the cue was played but liquid access was withheld (Fig. 5b).

We found that 58% of anterior BLA_{D1R} neurons were activated by sucrose ingestion with dynamics that were time-locked to the start of licking (Fig. 5c; peak time: 3.4±0.3s from the first lick in each bout; Extended Data Fig. 11b–c). In contrast, we observed only weak activation of these cells during mock trials (1.0±0.2z vs. 0.08±0.09z, sucrose vs. mock, p=1e-5), and these differences persisted when we controlled for the number of licks (Extended Data Fig. 11d–f), indicating these responses depend on ingestion. In addition, the responses to sucrose and sucralose were highly correlated, both at the level of individual neurons (p=7.7e-8; Fig. 5d–e; Extended Data Fig. 11g–i) and population dynamics (Fig. 5f; Extended Data Fig. 11j). In contrast, ingestion of water produced less activation and a distinct population trajectory (Fig. 5f; Extended Data Fig. 11h–j). Together, this demonstrates that many anterior BLA neurons specifically represent sweet tastes.

We next investigated how anterior BLA_{D1R} neurons respond to purely post-ingestive signals by recording their activity during and after IG infusion of sucrose. This revealed a slow ramping

activation during sucrose infusion that was not observed with sham, water or non-nutrititve mannitol infusion (Fig. 5g; Extended Data Fig. 11k–p). We observed a similar ramping activity following infusion of Intralipid or Ensure, confirming that these are bona fide nutrient responses.

We wondered how the phasic signal representing sweet taste and the tonic signal represent GI feedback are integrated in individual neurons. We reasoned that if learning happens in the anterior BLA, then nutrients might modulate the strength of BLA responses to gustatory signals Indeed, we found that responses to licking non-nutritive sucralose diminished during the course of the one session, whereas responses to sucrose were stable at the single-cell and population level (Fig. 5h–j; Extended Fig. 11q–r). This indicates that nutrient and gustatory responses converge on the same cells in anterior BLA, and that this integration strengthens responses to tastes associated with calories.

The integration of taste and post-ingestive signals in anterior BLA_{D1R} neurons suggests that these cells could be critical for learning about the nutrient content of food. To test their necessity, we optogenetically silenced anterior BLA_{D1R} neurons during flavor-nutrient conditioning, which completely prevented mice from learning which flavor was associated with calories (Fig. 5k–l; Extended Fig. 12a). Importantly, silencing these neurons did not result in a decrease in food intake when hungry animals were given Ensure (Extended Fig. 12c), indicating that anterior BLA_{D1R} neurons are not required for ingestion per se. However, silencing these neurons did decrease consumption of a non-caloric solution newly paired with IG glucose infusion (Extended Fig. 12b), indicating that they are important for updating the value of flavors when the nutrient content of food is uncertain. This effect was specific to flavor-nutrient learning, as inhibition of these neurons did not block a different form of post-ingestive learning, CFA (Extended Fig. 12d). Thus, anterior BLA_{D1R} neurons integrate flavor cues with nutrient signals to assign value to calorie-rich foods.

The left side of the brain preferentially responds to nutrients in mice and humans

All of the recordings described above were performed in the left amygdala. However, there have been reports that aversive stimuli, such as those that induce fear[39,40] and pain[41], preferentially engage the right amygdala. To test whether internal nutrient signals are differentially represented on the right and left hemispheres, we prepared mice for matched recordings in the right and left BLA during nutrient infusions. Remarkably, we found that there was greater DA release in left BLA compared to right following IG infusion of Ensure (18.2±3.5% vs 5.3±1.0%, p=5.3e-4; Fig. 6a; Extended Fig. 13a–b) or glucose (Extended Fig. 13c). Of note, the lateralized

260 responses in BLA were not due to a technical defect in our right hemisphere recordings, because the short-timescale DA release in response to licking was slightly greater on the right compared to the left (Fig. 6b; Extended Fig. 13d–g). To confirm this effect was not driven by between-subject variability, we recorded simultaneously from both hemispheres in a new cohort of mice (Extended Fig. 13h). This approach again revealed that IG nutrients evoke stronger DA
265 release in left BLA (Fig. 6c; Extended Fig. 13j–l), even though activity was comparable and tightly aligned across the two sides at baseline (Fig. 6d; Extended Fig. 13i). This demonstrates that ingested nutrients can be preferentially represented in one hemisphere of the mouse brain.

We wondered whether humans show similar lateralized responses. While dopamine responses to IG nutrient infusion have not been measured in humans, one study[42] reported dopamine
270 release (measured by 11C-raclopride PET) at fixed intervals during and after ingestion of a milkshake, enabling isolation of putative internal nutrient driven signals. Reanalysis of this data showed that, as in the mouse, the BLA is a major site of post-ingestive DA release in humans (Fig. 6e; Extended Fig. 14a–b). Moreover, this post-ingestive DA release was localized to the left BLA, specifically in the anterior portion, revealing that this small region is a hotspot for
275 nutrient-triggered DA in both mice and humans. In a separate experiment utilizing fMRI in humans, we found that there was increased activity in BLA following consumption of glucose compared to water, and this was again localized to the anterior BLA in the left hemisphere (Fig. 6f; Extended Fig. 14c). Thus, these data reveal that there is an evolutionarily conserved, dopaminergic pathway conveying nutrient signals preferentially to the left anterior BLA.

280 We considered two possible mechanisms that could give rise to these lateralized responses in BLA (Fig. 6g). One possibility is that they arise from asymmetric sensory inputs to the brain, which is suggested by data showing that there are functional differences between the left and right vagus nerve[16,43]. An alternative possibility is that lateralization is imposed by a top-down pathway, which is suggested by the fact that insular cortex, which is heavilly interconnected with
285 BLA, shows asymmetric responses to aversive visceral cues[44,45].

To test the first possibility, we removed the vagus from one side of the body and measured DA responses in the BLA. Mice were outfitted for simultaneous recordings of DA release in right and left BLA, and responses to IG nutrient infusion were recorded at baseline. We then performed a unilateral vagotomy, removing either the left or right vagus, and repeated these
290 recordings. We found that unilateral vagotomy reduced IG nutrient responses by approximately 50%, regardless of which vagus was severed, indicating that DA responses to nutrients involve the vagus (Extended Fig. 15). However, there was no differential response to left or right

vagotomy in either the left or right BLA (Fig. 6h–i), indicating that lateralized DA release in BLA does not originate from asymmetric vagal input.

To test the second possibility, we asked whether there are differences in the inputs to the right versus left VTA^{DA}—>BLA pathway, given that the two projections are ipsilateral and anatomically separable[46] (Extended Fig. 16a–e). To do this, we used a polysynaptic retrograde tracing approach in which we injected the Cre-dependent pseudorabies virus (PRV-Introvert-mCherry) into either the left or right BLA of DAT-Cre mice (Fig. 6j). This results in PRV being taken up by axon terminals in the BLA, transported retrogradely to DA neuron cell bodies in the VTA, and then spreading polysynaptically at a rate of approximately one synapse per day. Four days after injection, we performed brain-wide imaging and registration of labelled neurons to the standard mouse brain atlas[47] (CCFv3[48], which contains 372 brain regions), and then ranked these brain regions according to their differential labelling following right versus left BLA injection. Strikingly, we found that the most highly enriched structure was visceral cortex, a subdivision of the insula known to be functionally lateralized[44,45] (Fig. 6k–l); whereas no large differences were seen in the nucleus of the solitary tract, where vagal signals enter the brain (Extended Fig. 16f). Additionally, the top 10 regions included several interconnected higher-processing structures, including other subdivisions of the insula and amygdala (Fig. 6m; Extended Fig. 16g–l). This prioritizes further investigation of the insula-amgydala network to understand how lateralization arises.

Summary

Animals must learn which foods are nutritious based on their post-ingestive effects[1–4]. While these post-ingestive effects could in principle be associated with any sensory cue, there is much evidence that there is a privileged pathway connecting the flavor of food, sensed in the mouth, with its nutrient content sensed in the gut. For example, animals can readily learn to lick a flavored solution, but not press a lever, in order to receive an IG infusion of nutrients[5,6]. Similarly, animals will learn to prefer a place associated with IG nutrient infusion only if it is coupled with an orosensory cue[49]. This suggests that there is a hardwired pathway in the brain that connects flavors and nutrients in order to drive learning about food, but the underlying circuits have been unknown.

Here, we have shown that there is a genetically and anatomically-distinct pathway within the midbrain dopamine system that is responsible for associating nutrients and flavors. This pathway is defined by CCK-expressing VTA_{DA} neurons that relay internal nutrient signals to a

specific subregion of the amygdala, namely the anterior portion of the BLA on the left side of the brain. A variety of functional tests show that this pathway receives the specific GI signals known to drive flavor preference, and that the underlying neurons are necessary and sufficient for flavor learning. On the other hand, we show that striatal DA pathways, which have long been assumed to drive this process[16,18,50–55], neither respond to GI nutrients nor are sufficient to drive flavor learning. This identifies a circuit involving the BLA—which has previously been shown to drive other forms of associative learning[24,36,56–58]—as the key pathway for learning which foods are nutritious.

Learning about food involves making associations with both its nutrient content and its environmental context. The latter is known to be mediated by phasic DA release in NAc in response to reward-predicting exterosensory cues. A salient feature of this form of learning is that it is temporally precise, meaning that DA must be released within (at most) a few seconds of the cue[59,60]. In contrast, nutrient detection in the gut is inherently slow and, as we show, involves DA signals that ramp over tens of minutes in the BLA. Consistent with the distinct properties of these two pathways, we found that acute stimulation of NAc DA projections invigorated ongoing behavior, but delayed and prolonged stimulation did not drive flavor learning. Conversely, acute stimulation of BLA projections did not alter behavior, but delayed stimulation drove robust flavor learning. This suggests a hierarchy in which the BLA pathway drives (or permits[36]) flavor–nutrient associations, while other pathways (e.g., NAc) link those flavors to external cues.

A surprising feature of this BLA pathway is that it is lateralized to the left hemisphere in both mice and humans. This could account for the unexplained alterations in ingestive behavior observed in individuals with lesions to the left BLA[61–63]. While a few functions, such as speech processing in humans, are known to be localized to one side of the brain, the neural circuits that govern core survival behaviors such as feeding are generally thought to be symmetric. Our studies suggest that the asymmetry in BLA nutrient responses arises from a lateralized amygdala-insula network. As few studies of feeding behavior in rodents have examined the possibility that the underlying circuits are lateralized, it will be important in the future to determine the anatomic origin of this functional asymmetry in the BLA. More broadly, these findings raise the possibility that there is a general role for hemispheric specialization in the control of feeding behavior.

Methods

All experimental protocols using mice were approved by the University of California, San Francisco Institutional Animal Care and Use Committee, in accordance with the NIH *Guide for the Care and Use of Laboratory Animals*. Human experiments were approved by the ethics committee of the Medical Faculty of the University of Cologne, Germany (fMRI, No. 17-278; PET, No. 16-320).

For clarity, methods are organized into sections for surgery, recordings, behavior, and analysis. Each subsection specifies the species used (mouse or human).

Mouse strains

The following transgenic lines were used: *Drd1a-Cre* (MMRRC #030989), *DAT-Cre* (Jackson #006660), *CCK-Cre* (Jackson #012706), *Vglut2-Cre* (Jackson #016963), *Vgat-Cre* (Jackson #016962), *DAT-Flp* (Jackson #033673), *TiGRE-GCaMP7s* (Jackson #034112), *Rosa-GtACR1* (Jackson #033089), and *RosaFL-ReaChR* (Jackson #024846). *LepR-Cre* mice were obtained from Martin Myers. Double and triple mutant lines were generated through standard breeding.

SURGERY: General methods (mice)

Mice were anesthetized with 2% isoflurane and placed on a thermostatically controlled heating pad. Sustained-release buprenorphine (1.5 mg/kg, subcutaneous, or SC) and meloxicam (5 mg/kg, intraperitoneal, or IP) were administered preoperatively. Ophthalmic ointment was applied to the eyes, and surgical sites were shaved and sterilized with alternating betadine and ethanol. Local anesthesia was provided with 0.25% bupivacaine (SC) at the incision site.

SURGERY: Intragastric catheters (mice)

Sterile polyurethane catheters (C30PU-RGA1439, Instech Labs) were attached to vascular access buttons (VABM1B/22, Instech Labs). Catheters were inserted into the avascular wall of the stomach and externalized dorsally through the access button secured on the upper back. Mice recovered for at least one week before experimentation.

SURGERY: Unilateral vagotomies (mice)

Under isoflurane anesthesia, a midline ventral neck incision was made to expose the salivary glands, which were gently separated and retracted laterally. The sternomastoid, sternothyroid, and omohyoid muscles were then retracted to reveal the carotid triangle. The carotid sheath was carefully opened, and the vagus nerve isolated for transection (>2 mm segment removed) below the level of the superior laryngeal branch. The incision was immediately closed with absorbable sutures, and mice were allowed to recover. In rare cases, transient ipsilateral ptosis (Horner's sign) was observed, likely due to inflammation of the cervical sympathetic trunk; otherwise, the procedure was well tolerated without complications.

All recordings were performed within two weeks after surgery, and post-mortem inspection confirmed no visible nerve regrowth. In a subset of mice, intraperitoneal injection of WGA Alexa Fluor 555 was performed after experimental completion. One week later (3 weeks after surgery), nodose ganglia were dissected and examined, revealing labeling restricted to the ganglion contralateral to the vagotomy, confirming lasting nerve transection.

SURGERY: Intracranial injections (mice)

Mice were anesthetized with isoflurane and positioned in a stereotaxic apparatus (Kopf Instruments). The skull was leveled between bregma and lambda, and small burr holes were drilled above target regions. Viral vectors were delivered via pulled glass pipettes. Pipettes were left in place for >5 min after injection to prevent backflow, then raised 0.05 mm dorsoventrally to create slight negative pressure and held for an additional >5 min before withdrawal. Coordinates are given relative to bregma.

<u>Anterograde tracing.</u> (see Fig. 3b) *CCK-Cre × DAT-Flp mice were prepared for tracing VTA-DA/CCK terminals by injecting AAV9-Con/Fon-ChR2-GFP* (300 nL; 6.0 × 10^{12} vg/mL; provided by K. Yackle and I. Bachmutsky) *bilaterally into VTA* (−3.1 AP, ±0.5 ML, −4.5 DV). Mice were perfused three weeks later and their brains processed for histology. Direct injection into VTA was necessary here due to the presence of DA/CCK neurons in dorsal raphe and the periaqueductal grey, which project to CeA[1]. Note that tracing of VTA-DA/LepR terminals (see Fig. 3f) was accomplished instead with a genetic cross *LepR-Cre × DAT-Flp with RosaFL-ReaChR mice.*

<u>Rabies tracing.</u> (see Extended Fig. 16a–e) *DAT-Cre* mice were prepared for monosynaptic retrograde tracing by injecting AAV5-EF1α-FLEX-TVA-mCherry (400 nL; 4.9 × 10^{12} vg/mL; UNC

Vector Core) bilaterally into VTA (−3.1 AP, ±0.5 ML, −4.5 DV). Three weeks later, CVS-N2c-ΔG-mGFP (100 nL; 7.8 × 10^8 vg/mL; Janelia) was injected into the left anterior BLA (−1.0 AP, −3.0 ML, −4.8 DV). Mice were perfused one week later and brains processed for histology.

Pseudorabies tracing. (see Fig. 6j–m; Extended Fig. 16f–l) *DAT-Cre* mice received PRV-Introvert-GFP (150 nL; 4.7 × 10^9 vg/mL; Princeton) into either the left or right BLA (−1.7 AP, ±2.9 ML, −4.8 DV) for polysynaptic retrograde tracing. Mice were perfused 1–5 days after injection. Labeling first appeared in ipsilateral VTA (day 1), expanded within VTA by day 2, and reached bilateral hypothalamic nuclei (LH, PVH) by day 3. On day 4, labeling bilaterally extended to cortical, amygdalar, and hindbrain regions. By day 5, animals displayed systemic illness, and labeling had spread to both nodose ganglia. All analyses used brains collected 4 days post-injection—the latest stage showing extensive labeling with minimal distress.

SURGERY: Intracranial implants (mice)

Following viral injection, optical fibers or GRIN lenses were implanted 0.1–0.15 mm above the target site and secured with dental cement (Metabond). A custom titanium headplate (eMachineShop) was attached with the GRIN lens to accommodate our 2-photon imaging set up.

For miniscope imaging, a second surgery was performed 4 weeks after virus injection to install a baseplate (Inscopix 100-000279) above the GRIN lens. The baseplate was affixed with dental cement and protected with a removable cover (Inscopix 100-000241).

Dopamine imaging. (see Figs. 2, 3, 6 and Extended Figs. 2–6, 9, 13, 15) Wild-type mice were injected with AAV9-hSyn-GRAB-DA3m (200 nL; 4–8 × 10^{12} vg/mL; WZ Biosciences) and implanted with an optical fiber (Doric MFC_400/430-0.48_6 mm_MF2.5_FLT) at the following injection coordinates:

- Left DLS (+1.5 AP, -1.5 ML, −3.0 DV)
- Left NAc core (+1.4 AP, −1.0 ML, −4.5 DV)
- Left or right BLA (−1.7 AP, ±2.9 ML, −4.8 DV)
- Left lateral BLA (−1.7 AP, −3.2 ML, −4.8 DV)
- Left anterior BLA (−1.0 AP, −3.0 ML, −4.8 DV)
- Left posterior BLA (−2.4 AP, −3.3 ML, −4.7 DV)

Simultaneous bilateral recordings used dual injections and fiber implants in the same animal.

For region-specific recordings (see Fig. 3 and Extended Fig. 9), *Vglut2-Cre* mice (BLA) and *Vgat-Cre* mice (CeA) were injected with AAV9-hSyn-DIO-GRAB-DA3m (200 nL; 8.8 × 10^{12} vg/mL; WZ Biosciences) and implanted with fibers above left BLA (−1.7 AP, −2.9 ML, −4.8 DV) or left CeA (−1.5 AP, −2.65 ML, −4.5 DV).

VTA-DA neuron imaging. (see Fig. 3a and Extended Fig. 7a–c) For VTA-DA population imaging, *DAT-Cre* mice received AAV1-FLEX-CAG-jGCaMP7s (300 nL; 6.3 × 10^{12} vg/mL; Addgene 104495) into left VTA (−3.1 AP, −0.5 ML, −4.5 DV), followed by implantation of a GRIN lens (8.4 × 0.5 mm, Inscopix 1050-004629) positioned 0.15 mm above the target.

For subpopulation imaging (see Fig. 3b–h and Extended Figs. 7d–o, 8), *CCK-Cre* × *DAT-Flp* × *RosaFL-GCaMP7s* mice (for VTA-DA/CCK) and *LepR-Cre* × *DAT-Flp* × *RosaFL-GCaMP7s* mice (for VTA-DA/LepR) underwent the same GRIN lens implantation above left VTA (−3.1 AP, ±0.5 ML, −4.5 DV).

BLA-D1R neuron imaging. (see Fig. 5a–j and Extended Fig. 11) For recording anterior BLA neurons, *Drd1a-Cre* mice were injected with AAV1-CAG-FLEX-GCaMP8s (200 nL; 5.9 × 10^{12} vg/mL; HHMI Janelia) into left aBLA (−1.0 AP, −3.0 ML, −4.8 DV) and implanted with a GRIN lens (8.4 × 0.5 mm, Inscopix 1050-004629) 0.15 mm above the injection site.

VTA-DA projection stimulation. (see Fig. 4 and Extended Fig. 10) For optogenetic activation of VTA dopamine terminals, *DAT-Cre* mice were injected with AAV1-EF1α-DIO-hChR2(H134R)-mCherry (300 nL; 6.0 × 10^{12} vg/mL; Addgene 20297) into left and right VTA (−3.1 AP, ±0.5 ML, −4.5 DV). For optogenetic activation of dopamine terminals in DLS, *DAT-Cre* mice were injected with AAV1-EF1α-DIO-hChR2(H134R)-mCherry (300 nL; 6.0 × 10^{12} vg/mL; Addgene 20297) in both bilateral VTA (−3.1 AP, ±0.5 ML, −4.5 DV) and bilateral substantia nigra (−3.1 AP, ±1.5 ML, −4.5 DV).

Paired optical fibers (200 μm, Thorlabs CFLC230-10) were implanted bilaterally 0.1 mm above downstream projection targets, including NAc (+1.4 AP, ±1.0 ML, −4.5 DV), aBLA (−1.0 AP, ±3.0 ML, −4.8 DV), pBLA (−2.4 AP, ±3.3 ML, −4.7 DV), CeA (−1.5 AP, ±2.65 ML, −4.5 DV), and DLS (+1.5 mm AP, -1.5 mm ML, -3.0 mm DV).

470 Control mice received AAV1-hSyn-DIO-mCherry (300 nL; 5.7 × 10^{12} vg/mL; Addgene 50459) instead of ChR2.

VTA-DA and aBLA-D1R neuron inhibition. (see Figs. 1, 5 and Extended Fig. 1, 12) For VTA-DA inhibition, *DAT-Cre* × *Rosa-GtACR* mice (and littermate controls) were implanted with bilateral fibers (Doric DFC_200/245-0.37_5 mm_GS1.0_FLT) 0.1 mm above VTA (−3.1 AP, ±0.5 ML,
475 −4.5 DV).

For aBLA-D1R inhibition, *Drd1a-Cre* × *Rosa-GtACR* mice (and controls) were implanted with bilateral 200 μm fibers (Thorlabs CFLC230-10) 0.1 mm above aBLA (−1.0 AP, ±3.0 ML, −4.8 DV).

RECORDINGS: General methods (mice)

480 Except where noted, recordings were performed in sound-isolated behavioral chambers (Coulbourn Habitest Modular System). Chambers were cleaned between sessions to remove residual olfactory cues. Mice were habituated to the chamber for ≥1 h with recording equipment and intragastric (IG) catheters attached before the first experimental day, and for 10–20 min before each subsequent session. When used for imaging, the excitation LED was turned on
485 during habituation to reduce bleaching artifacts. Except when noted, mice were sated (not food/water deprived).

For recordings of BLA neuron dynamics, mice were head-fixed using the custom titanium headplate (eMachineShop, see surgery methods above) above a miniature treadmill. These mice were habituated for at least three 1 hour sessions, then re-habituated for 10–20 min before
490 each recording. Both sexes were used in approximately equal numbers.

Lick-evoked responses were recorded while mice consumed specific solutions after 18–24 hours of water or food deprivation. Water-restricted mice received water, 32% sucrose or 0.8% sucralose (matched for perceived sweetness to sucrose solution); food-restricted mice received 35% Ensure (isocaloric to sucrose solution). Each session began with a 10-min baseline period
495 followed by access to a lickometer spout. Mice were first habituated to the setup with 1 h access to sucralose while attached to the camera.

For imaging of BLA neuron dynamics, mice were trained to lick 32% sucrose in response to a 5-s 2 kHz tone cue. After three training sessions, recordings were performed over three

consecutive days, each presenting water, sucrose, or sucralose in counterbalanced order
500 across mice. Animals were presented with 50 or 120 cue trials, separated by 20 seconds (lasting 1250 or 3000 seconds, respectively). During these recording sessions, 10% of cues omitted liquid delivery to isolate licking-only trials (these no-delivery trials are called “mock” trials).

IG-evoked responses were recorded by infusing solutions through previously implanted
505 catheters at 100 µL/min for 10 min (Harvard Apparatus 70-2001 syringe pump). Tubing (AAD04119 Tygon, LS20/PNP3M Instech) was connected before habituation. Infusions began after a 10-min baseline.

For receptor-blockade experiments, antagonists were mixed into the infused solution: 600 µg/mL mizagliflozin (SGLT1), 50 µg/mL GW1100 (GPR40), 50 µg/mL AH7614 (GPR120), or 10
510 µg/mL sulfo-N-succinimidyl oleate (CD36). For CCK blockade, 1 mg/kg devazepide (in saline, 10 mL/kg IP) was administered 30 min prior to infusion.

Sugar infusions (sucrose, glucose, fructose, galactose, MDG, mannitol) were 32% w/v; sucralose was 0.8%. Other nutrient solutions were isocaloric to 32% sucrose: 35% Ensure, 32% collagen peptide, 14% intralipid, diet A (17.3% sucrose + 4.5% intralipid + 4.5% peptide), and
515 diet B (6.5% sucrose + 8.5% intralipid + 6.4% peptide). Controls used 14% mineral oil or double-distilled water.

Hormone-evoked responses were elicited after a 10-min baseline by IP injection of saline (10 mL/kg) containing 2 mg/kg serotonin HCl, 10–30 µg/kg cholecystokinin octapeptide, 100 µg/kg peptide YY, 2 mg/kg ghrelin, 2 mg/kg glucagon, or 10 µg/kg amylin.

520 Visceral malaise was induced by IP injection of saline containing lithium chloride (100 mg/kg) or lipopolysaccharide (200 µg/kg) after the same baseline period.

RECORDINGS: Photometry (mice)

Fluorescence signals were acquired using continuous 470 nm and 420 nm excitation (40 µW per LED; RZ10X LUX-I/O, TDT). Signals were sampled at 1.0173 kHz using Synapse (TDT) and
525 exported via Browser (TDT). Raw traces were downsampled to 4 Hz in MATLAB for analysis.

RECORDINGS: Miniscope videos (mice)

Miniscope recordings were acquired at 8 Hz (0.2 mW/mm², 455 nm LED, gain = 8, 2× spatial downsampling) using an *nVista 3.0* system (Inscopix DA 2.0). Videos were pre-processed by spatial (2×) and temporal (2×) downsampling, bandpass filtering, and motion correction in Inscopix Data Processing 1.9. Sessions were excluded if motion exceeded the average neuron diameter after correction.

Cell activity was extracted using CNMF-E implemented in MATLAB (github.com/zhoupc/cnmfe). Segmented ROIs were manually refined to remove motion artifacts, duplicates, and over-segmented regions. Cells exhibiting bleaching artifacts fit by an exponential decay during baseline were excluded.

RECORDINGS: 2-photon videos (mice only)

Two-photon imaging was performed at 20 Hz (512 × 512 pixels, 900 nm excitation; Chameleon Discovery laser, Coherent) with a resonant-galvo scanner (Ultima Investigator, Bruker PV 5.8). Videos were spatially (2×) and temporally (2×) downsampled, bandpass-filtered, and motion-corrected using Inscopix Data Processing 1.9, followed by additional correction and ROI extraction using EZcalcium[2] built on NoRMCorre[3] and CaImAn[4] toolboxes (https://github.com/porteralab/EZcalcium). ROIs were manually curated with CaImAn refinement and cross-registered across sessions using custom code based on the CaImAn ROI-matching module.

RECORDINGS: fMRI imaging (humans)

To test whether glucose consumption modulates BOLD activity in the human basolateral amygdala (BLA), overnight-fasted participants performed a *Drink Task* during fMRI (MAGNETOM Prisma Fit, Siemens AG, Medical Solutions, Erlangen, Germany). Testing began with a subjective state rating, standardized task instructions, and a blood draw. Participants were then positioned in the scanner, where two bottles—one containing 300 mL of 28% w/v glucose monohydrate (equivalent to 25% w/v glucose) and one containing water—were placed behind the head coil and connected via two plastic tubes resting on the participant's chest (the glucose tube marked with tape).

The scan began with a 2-min baseline during which a fixation cross was shown. Participants were then instructed (via on-screen text) to grasp the marked tube, drink the glucose solution, and press a response key with their right index finger (Response Pad, Current Designs). After

ingestion, they rated sweetness and palatability on visual analogue scales (0 = not at all, 100 = very). They then drank water from the second tube until the taste was neutral and confirmed completion with a key press. A fixation cross was shown for the remaining 20-min scan period. The procedure was conducted on a computer using MATLAB (R2019b) and Psychophysics Toolbox (PTB-3 v3).

The total task duration was approximately 25 min, varying slightly between participants due to self-paced drinking. Thirty-eight healthy participants were included in the analysis (19 female; mean age, 29.2 ± 6.4 years; mean fasting duration, 12.0 ± 1.7 h).

RECORDINGS: PET imaging (humans)

This protocol was previously published[5], and the existing dataset was reanalyzed for the present study. Thirteen healthy male participants underwent positron emission tomography (PET) using a Siemens HRRT scanner while receiving one of two oral stimuli: a milkshake or a tasteless noncaloric control solution. To measure dopamine release, participants were injected intravenously with 220–370 MBq [^{11}C] raclopride via a programmable syringe pump (Perfusor Compact, Braun Melsungen). Seventy percent of the tracer dose was delivered within the first minute, with the remaining 30% infused slowly over the following 59 min. Each session lasted 60 min, during which participants remained awake and motionless.

Each subject participated in two sessions (one with milkshake and one with the control solution) on separate days following a 10–11 h overnight fast.

BEHAVIOR: General methods (mice)

All behavioral assays were conducted in sound-attenuated chambers (Coulbourn Habitest Modular System). Chambers were cleaned between sessions to remove residual olfactory cues. Mice were habituated for at least 1 h to the chamber—with all recording equipment and intragastric (IG) catheters attached—before the first experimental day, and for 10–20 min before each subsequent session. Both sexes were used in approximately equal numbers for all experiments. Experimenters were blinded to group identity (e.g., ChR2 vs. mCherry).

For optogenetic manipulations, light was delivered using a 473-nm DPSS laser (Shanghai Laser and Optics Century, BL473-100FC) connected via patchcords (MFP_200/220/900-

585 0.22_2m_FCM-ZF1.25 or SBP_200/220/900-0.22_2m_FCM-GS1.0, Doric). Laser power was calibrated daily and set to 1–2 mW for inhibition and 10–15 mW for activation.

BEHAVIOR: Flavor-nutrient conditioning (mice)

Mice underwent a 9-day flavor–nutrient conditioning paradigm (2 pre-training test days, 6 training days, 1 post-training test day) while maintained at 85–90% of initial body weight. During
590 pre- and post-tests, mice were given 1 h two-bottle choice assays offering 0.2% saccharin solutions flavored with 0.1% Lemon–Lime or Grape Kool-Aid (Kraft Foods). Bottle positions were randomized and counterbalanced across test days.

During training, mice were attached to IG catheters and allowed 1 h access to one flavored solution, which triggered a 1 μL/lick IG infusion. Four counterbalanced groups associated one
595 flavor with 8% glucose infusion and the other with water, with infusion order reversed between groups. Mouse assignment to each group was randomized, except that animals with >90% initial preference for the flavor paired with glucose infusion were excluded to avoid pre-existing bias (analyses without these mice are included in Extended Data Table 1). Mice were removed if body weight dropped below 85% or if catheters, patch cords, or cannulae disconnected during
600 training.

Optogenetic silencing during conditioning was achieved with continuous 1–2 mW illumination in mice prepared for VTA-DA or BLA-D1R inhibition.

Optogenetic activation was achieved with 10–15 mW, 10 Hz stimulation (1 ms pulses; 2 s ON, 3 s OFF; 12 cycles) delivered after each lick following a 20 s delay, in mice prepared for VTA-DA
605 terminal activation. In these sessions, no glucose or water was infused.

BEHAVIOR: Conditioned flavor avoidance (mice)

Mice underwent a 3-day conditioned flavor avoidance (CFA) protocol (2 training days and 1 test day). Mice were water-deprived for 24 h before each training or testing session, with a 1-week recovery period between days. On training days, mice were given 1 h access to a 5% sucrose
610 solution flavored with 0.2% Orange or Cherry Kool-Aid (Kraft Foods). Prior to training, mice were naïve to both sucrose and these flavors. Ten minutes after the first lick bout, each mouse received an intraperitoneal injection of lithium chloride (100 mg/kg in saline). Mice were then returned to the chamber with continued solution access for the remainder of the session.

On the test day, mice were given simultaneous access to two bottles—one containing water and
615 the other containing the previously flavored sucrose solution—to assess preference. Bottle positions (front vs. back) were randomized across mice. Licks were recorded using a lickometer integrated into the Coulbourn Habitest system. Mice were excluded if patchcords or cannulae disconnected during training.

Optogenetic silencing during CFA was performed with continuous 1–2 mW illumination in mice
620 prepared for VTA-DA or BLA-D1R inhibition.

Optogenetic activation was performed in VTA-DA terminal activation mice using 10–15 mW, 10 Hz laser pulses (1 ms pulse width; 2 s ON, 3 s OFF) delivered after the first lick following a 20 s delay, continuing for the remainder of the session. In this condition, no LiCl injection was administered.

625 **BEHAVIOR: Lever pressing assays (mice)**

Mice were trained to self-stimulate VTA-DA terminals using optogenetic activation. Stimulation was delivered through implanted cannulae connected to a 10–15 mW, 473-nm laser as described above. Mice underwent a 3-day lever-pressing protocol in which they had access to two levers for 1 h per day. Pressing one lever triggered terminal stimulation (20 Hz, 1 ms pulse
630 width, 5 s total). The position of the active lever (front vs. back) was randomized on the first day and held constant thereafter. Mice were excluded if patchcords or cannulae disconnected during any session.

BEHAVIOR: Feeding assays (mice)

In a set of related assays, mice were given access to flavored Ensure solutions during
635 optogenetic inhibition or activation. On four separate days, mice were provided 30 min access to a flavored Ensure solution following 1 h of water and food deprivation. Two sessions were conducted with the laser off and two with the laser on, in counterbalanced order. Consumption was averaged across replicate “laser on” and “laser off” sessions. Testing time was kept consistent (±30 min) to control for circadian effects.

640 Optogenetic silencing during feeding was achieved with continuous 1–2 mW illumination in mice prepared for VTA-DA or BLA-D1R inhibition. The laser remained on throughout access to a

vanilla Ensure solution. If patchcords or cannulae disconnected during a “laser on” session, data from that day were discarded and the session repeated if possible.

Optogenetic activation during feeding was performed in mice prepared for VTA-DA terminal activation. Three flavored Ensure solutions (vanilla, chocolate, strawberry) were tested in separate assays:

- Continuous stimulation – 10 Hz, 1 ms pulses (2 s ON, 3 s OFF) delivered during access to vanilla Ensure.
- Lick-terminated stimulation – same parameters, but laser turned off for 2 s following each lick (chocolate Ensure).
- Lick-triggered stimulation – same parameters, but laser turned on for 2 s after each lick (strawberry Ensure or water).

If cannulae disconnected during any “laser on” day, data were discarded and the session re-run if possible.

ANALYSIS: Recordings (mice)

All analyses were performed using custom MATLAB scripts (R2023a). Unless otherwise stated, data are presented as mean ± SEM, with shaded areas in line plots indicating SEM or 95% confidence intervals for regression fits. Except where noted (e.g., linear regressions, Kolmogorov–Smirnov tests), all statistical comparisons used nonparametric two-sided permutation tests (100,000 iterations or exact when possible). One-sided tests were applied sparingly, in cases where directionality was pre-specified, specifically in two cases: (1) in conditioned flavor avoidance experiments, where activation or LiCl injection could only decrease sucrose preference since it can be near 100% at baseline (2) in self-stimulation experiments, where activation could only increase lever pressing since it can be near 0 at baseline.

ANALYSIS: Time windows (mice)

Activity was analyzed across three standardized time windows:

- Oral phase: 0–5 s after the first lick in a bout. Lick bouts were defined as clusters of licks separated by ≤2 s and lasting ≥2 s. Only the first bout was analyzed (except in 2-photon recordings), as post-ingestive signals are minimal during this period. Given that mice

670 consume ~9.6 μL/s[6] and swallow at ~1 Hz[7], a 5 s bout maximally represents ~38 μL swallowed (≈10% of baseline stomach volume[8]), consistent with minimal GI feedback.

- IG phase: 20–600 s after the start of intragastric (IG) infusion, corresponding to the arrival of solution in the stomach (~20 s transit) and continuing through the 10 min infusion period.
- 675 Post-IG phase: 1200–3000 s after infusion onset (10–40 min post-infusion), allowing for fluid clearance from the stomach and intestinal transit (which based on oral gavage studies exceeds 5 min[9]).
- Hormone phase: 0–300 s after intraperitoneal (IP) injection. Useful for quantifying immediate responses to systemic injection.
- 680 Malaise phase: 300–1800 s after IP injection. This time window was only used for LPS responses, owing to delayed action.

ANALYSIS: Photometry (mice)

Fluorescence signals were acquired at isosbestic (420 nm) and activity-dependent (470 nm) wavelengths. The activity-dependent signal was normalized to the isosbestic trace to remove
685 motion artefacts using $\Delta F/F_0 = (F - F_0)/F_0$, where F_0 was predicted from a linear regression of the two signals during the 10 min baseline. For IG and IP manipulations, each recording was further normalized by subtracting the corresponding sham or saline trace from the same mouse. Un-subtracted traces are shown in example figures, while subtracted traces were used for statistics and summary plots.

690 To account for relative differences in DA axon density, we normalized photometry traces by z-scoring relative to baseline activity during drinking in Fig. 2. The raw $\Delta F/F_0$ activity for this experiment can be found in the supplement (Extended Fig. 4).

ANALYSIS: Single-cell imaging (mice)

Neural activity traces were extracted after CNMF-E segmentation (see Recording Methods) and
695 z-scored relative to baseline activity. Lick timing was aligned to neural traces via TTL signals. For miniscope data, only the first lick bout was analyzed; for 2-photon recordings, all bouts were combined (typically <5 s each, separated by >20 s).

Sham sessions and control distributions. To control for baseline drift and intrinsic excitability differences across neurons and animals, we recorded “sham” sessions in which mice were

700 placed in the behavioral chamber but received no stimulation, infusion, or reward. These sessions were used to generate empirical distributions of spontaneous neuronal activity for each time window. For lick-related analyses, TTL timestamps from real licking sessions (e.g., Ensure or sucrose) were applied to sham recordings to create matched sham lick responses.

Activated and inhibited thresholds. Neurons were classified as activated or inhibited using
705 empirical thresholds derived from sham distributions, rather than fixed z-score cutoffs. A neuron was considered activated if its z-scored activity exceeded the 95th percentile of its sham distribution and inhibited if below the 5th percentile (α=0.05).

This empirical approach was adopted because fixed ±1z thresholds, commonly used in the field (and in our prior work[10]), assume homogeneous baseline variance across neuron types and
710 timescales—an assumption that does not hold for mixed populations or long recordings. By contrast, this sham-based method defines activation relative to each neuron population's own spontaneous activity, thereby controlling for intrinsic excitability, drift, and noise.

Because baseline variance differed across time windows, independent thresholds were computed for each phase (e.g., IG vs. post-IG). For instance, 5% of VTA-DA/CCK neurons
715 exceeded +0.54 z during sham IG infusions and +0.69 z during sham post-IG periods. Distinct z-score thresholds were similarly derived for each neuron group (e.g., VTA-DA/LepR vs. VTA-DA/CCK) to control for differences in baseline excitability. Sham-derived distributions for licking responses were used in the same way to determine activation and inhibition cutoffs.

Cross-registration for neurons across days and conditions was performed manually. This was
720 achievable due to the sparsity of VTA-DA/CCK, VTA-DA/LepR, and aBLA-D1R neuron subpopulations.

Rise times for dopamine release were calculated from individual traces during IG infusions using a window from 1 minute before infusion onset to 5 minutes after. For lick response rise times, the window was the 5 seconds before and after lick bout onset. Traces were fitted with a
725 sigmoid curve, and the time at which the fit reached 5% of its final value was defined as $T_{5\%}$. The first time point exceeding baseline fluorescence by 3 standard deviations (σ, defined during baseline) was defined as $T_{3\sigma}$. Both metrics are shown unadjusted in Extended Data Table 2.

For comparisons reported in the text, catheter transit time was subtracted to yield adjusted rise times. Adjusted $T_{5\%}$ and $T_{3\sigma}$ values were averaged to compute the reported mean rise time, with standard errors combined as $\overline{SE} = \frac{\sqrt{\overline{var}}}{\sqrt{n}}$. Individual neuron recordings could not always use both rise-time measures: IG responses did not consistently follow a sigmoid function (so only $T_{3\sigma}$ was used), whereas lick-related responses rarely exceeded 3σ (so only $T_{5\%}$ was used). Consequently, rise times for neural activity and dopamine release were compared using the same metric within each analysis (e.g., IG responses using $T_{3\sigma}$).

Fall times were calculated analogously, using a window from 5 minutes before the end of infusion to 40 minutes after infusion offset.

Peak times for dopamine release during licking was determined from the first lick bout (0–30 s window from bout onset), defined as the time of maximal fluorescence within this period. For aBLA neuron activity, peak timing was measured in a shorter 0–5 s window after lick-bout onset, corresponding to the briefer access period.

Statistical corrections for between-subject variance were utilized when noted, with a linear mixed-effects model that treated individual mice as random effects. Intra-class correlations (ICC) were computed as $ICC = \frac{var(mice)}{var(total)}$ to quantify variance attributable to inter-animal differences. Where appropriate (e.g., Extended Fig. 11l), activity traces were also averaged by mouse to visualize ICC effects.

Clustering analyses were performed using principal component analysis (PCA) and k-means clustering. Traces were first downsampled (to 1 Hz for IG responses or 4 Hz for lick responses) and normalized by their absolute maximum. PCA was performed using MATLAB's built-in pca function with centering by singular value decomposition. The number of components plotted was determined by the elbow criterion on the scree plot (when unclear, the first 2 PCs were plotted alone). k-means clustering was implemented using MATLAB's kmeans function, with cluster number chosen by the silhouette method. Cluster assignments were then visualized using the unnormalized data.

ANALYSIS: fMRI recordings (humans)

All fMRI preprocessing and analyses were performed using SPM12 (Wellcome Trust Centre for Neuroimaging) and FSL (version 5.0.10) implemented in MATLAB (R2022b). Functional data were motion- and distortion-corrected (mcflirt[11], topup[12]), co-registered to individual structural images, normalized to MNI space using unified segmentation, and spatially smoothed with a 6 mm FWHM Gaussian kernel. The first 10 volumes were discarded to allow for magnetic stabilization.

Nuisance regressors included 24 motion parameters (current and preceding volume and their squares[13]), mean ventricular CSF signal, and motion-outlier volumes (> 1 mm framewise displacement[14]). Low-frequency drifts were high-pass filtered at 128 s.

We modeled the Drink Task using a mass-univariate general linear model (GLM). The baseline (2 min) and ten consecutive 2 min post-ingestion time bins were modeled as separate boxcar regressors convolved with the canonical hemodynamic response function and its time and dispersion derivatives. The drinking and rinsing phases were modeled as an additional regressor of variable duration, with all nuisance regressors included at the first level. Ten contrasts (post-ingestion > baseline) were computed for each subject.

Second-level analyses used a flexible factorial GLM including subject and condition factors, with sex, hunger rating, outside temperature, and insulin sensitivity (HOMA-IR) as covariates. Significance was assessed within anatomically defined left and right BLA masks (Trutti et al., 2021; threshold = 0.1) at $p < 0.05$, FWE-corrected at the peak level (initial voxel threshold = 0.05 uncorrected).

ANALYSIS: Behavior (mice)

Behavioral data were analyzed from Coulbourn system outputs of licking and lever pressing. Lick data are shown as cumulative totals or as flavor preferences, calculated as the percent preference for the flavor paired with neuronal stimulation, glucose infusion, or LiCl injection: $\frac{A}{A+B}$, where A is the total number of licks for one flavor and B for the other.

Lever-pressing behavior is shown as the difference between active and inactive lever presses. Statistical tests were corrected for multiple comparisons using the Benjamini–Hochberg

procedure, where n denotes the number of brain regions tested (see Fig. 4 and Extended Data
785 Fig. 10 and Extended Data Table 2).

ANALYSIS: Histology (mice only)

Mice were transcardially perfused with phosphate-buffered saline (PBS) followed by 10% formalin. Brains were post-fixed overnight at 4 °C, cryoprotected in 15% and then 30% sucrose (24 h each), embedded in OCT (Tissue-Tek), and sectioned on a cryostat (50 µm).

790 For immunostaining, free-floating sections were washed (3 × 5 min in PBS-T, 0.1% Triton X-100), blocked for 2 h at room temperature (2% normal goat serum + 3% BSA in PBS-T), and incubated for 12–48 h at 4 °C with primary antibodies in blocking solution. Sections were washed, incubated with fluorescent secondary antibodies for 2 h at room temperature, washed again, and mounted with DAPI Fluoromount-G (Southern Biotech). Images were acquired on an
795 Eclipse Ti2 inverted microscope (Nikon) and minimally processed in ImageJ (v1.53t).

Primary and secondary antibodies included: chicken anti-GFP (Abcam ab13970, 1:500) + goat anti-chicken Alexa 488 (Abcam ab150169, 1:500), and rabbit anti-RFP (Abcam ab124754, 1:500) + goat anti-rabbit Alexa 568 (Abcam ab175471, 1:500).

Fiber placement and viral spread were verified visually to generate anatomical placement maps;
800 median A–P slices are shown for each group. Because ML/DV coordinates vary along the A–P axis, some tracts on this median slice may appear slightly displaced. Mice with clear off-target fiber placements were excluded from analysis.

Pseudorabies retrograde tracing. Labeling from pseudorabies retrograde tracing was quantified using the QUINT semi-automated whole-brain analysis pipeline[15], which integrates image
805 registration, segmentation, and region-based cell counting across the Allen CCFv3 atlas. This produced quantitative “load” measurements (GFP^+ cells per unit area) for each of the 1,328 annotated brain regions. Segmentation and registration accuracy were manually validated in representative sections from each animal. Regions smaller than 100 pixels in any dimension and non-gray-matter annotations were excluded to avoid artefactual load estimates. Loads were
810 normalized to VTA labeling to control for viral transfection efficiency, ranked by difference following left vs right BLA injections, and visualized as force-directed graphs, dendrograms, and heat maps using connectivity matrices (0–5 scale) derived from literature curation.

Rabies retrograde tracing. GFP^+ cells were manually counted from five representative midbrain sections in each of three mice.

815

ANALYSIS: Graphing

For visualization, fluorescence and activity traces were down-sampled and smoothed using a moving-average filter (kernel size = 2). Long-duration traces (e.g., IG responses) were down-sampled to 0.1–0.2 Hz, whereas short-duration traces (e.g., licking responses) were down-
820 sampled to 1 Hz. Principal component (PC) space plots of licking activity were maintained at 4 Hz to preserve temporal resolution.

In some cases, the same dataset was visualized in multiple figures for distinct comparisons (e.g., dopamine responses during Ensure IG infusion in left BLA are shown in Fig. 2a, 6a, and Extended Fig. 3b to compare responses with striatum, contralateral BLA, and water infusion,
825 respectively).

Acknowledgements

We thank K. Yackle and I. Bachmutsky for providing *AAV-Con/Fon-ChR2 viruses.* We thank A. MacDonald for his help establishing the vagotomy method. This work was supported by the
830 National Institutes of Health grants R01-DK106399, R01-DK138127, R01-NS116626, and R01-DK145100 (to Z.A.K.) and F31-NS120468 (to J.C.R.G.). Z.A.K. is an Investigator of the Howard Hughes Medical Institute.

Author Contributions

835 J.C.R.G., D.M.S., M.T and Z.A.K. designed experiments and interpreted data. J.C.R.G. and L.Q. performed intragastric surgeries. J.C.R.G. performed intracranial and vagotomy surgeries. J.C.R.G. and Q.L. performed optogenetic experiments. J.C.R.G. and Q.L. performed photometry experiments. H.B., M.T., and D.M.S. performed and analyzed PET experiments. B.K. and M.T. performed and analyzed fMRI experiments. J.C.R.G. performed miniscope, 2-
840 photon, and other behavioral experiments. J.C.R.G., A.M.H., J.Z., J.C., V.U., Z.L. performed histological experiments. J.C.R.G. and A.M.H analyzed histological experiments. J.C.R.G.

analyzed optogenetic, photometry, miniscope, 2-photon, and other behavioral experiments. J.C.R.G and Z.A.K. wrote the manuscript with input from D.M.S. and M.T.

845 **Competing Interests**

The authors declare no competing interests.

Bibliography

850 1. Sclafani, A. Learned controls of ingestive behaviour. *Appetite* **29**, 153–158 (1997).

2. Capaldi, E. D. Conditioned Food Preferences. in *Psychology of Learning and Motivation* (ed. Medin, D. L.) vol. 28 1–33 (Academic Press, 1992).

3. Havermans, R. C. & van den Heuvel, E. 10 - Acquired tastes: on the learning of human food preferences. in *Flavor (Second Edition)* (eds Guichard, E. & Salles, C.) 283–299 (Woodhead

855 Publishing, 2023). doi:10.1016/B978-0-323-89903-1.00005-0.

4. Rozin, P. & Zellner, D. The role of Pavlovian conditioning in the acquisition of food likes and dislikes. *Ann. N. Y. Acad. Sci.* **443**, 189–202 (1985).

5. Sclafani, A. Conditioned food preferences. *Bull. Psychon. Soc.* **29**, 256–260 (1991).

6. Holman, G. L. Intragastric reinforcement effect. *J. Comp. Physiol. Psychol.* **69**, 432–441

860 (1969).

7. Azzara, A. V., Bodnar, R. J., Delamater, A. R. & Sclafani, A. D1 but not D2 dopamine receptor antagonism blocks the acquisition of a flavor preference conditioned by intragastric carbohydrate infusions. *Pharmacol. Biochem. Behav.* **68**, 709–720 (2001).

8. Touzani, K., Bodnar, R. J. & Sclafani, A. Dopamine D1-like receptor antagonism in amygdala

865 impairs the acquisition of glucose-conditioned flavor preference in rats. *Eur. J. Neurosci.* **30**, 289–298 (2009).

9. Touzani, K., Bodnar, R. & Sclafani, A. Activation of dopamine D1-like receptors in nucleus accumbens is critical for the acquisition, but not the expression, of nutrient-conditioned flavor preferences in rats. *Eur. J. Neurosci.* **27**, 1525–1533 (2008).

870 10. Zukerman, S., Ackroff, K. & Sclafani, A. Post-oral glucose stimulation of intake and conditioned flavor preference in C57BL/6J mice: A concentration–response study. *Physiol. Behav.* **109**, 33–41 (2013).

11. Zimmerman, C. A. *et al.* A neural mechanism for learning from delayed postingestive feedback. *Nature* **642**, 700–709 (2025).

875 12. Garcia, J., Ervin, F. R. & Koelling, R. A. Learning with prolonged delay of reinforcement. *Psychon. Sci.* **5**, 121–122 (1966).

13. Garcia, J., Lasiter, P. S., Bermudez-Rattoni, F. & Deems, D. A. A General Theory of Aversion Learning. *Ann. N. Y. Acad. Sci.* **443**, 8–21 (1985).

14. Grove, J. C. R. *et al.* Dopamine subsystems that track internal states. *Nature* **608**, 374–

880 380 (2022).

15. Alhadeff, A. L. *et al.* Natural and Drug Rewards Engage Distinct Pathways that Converge on Coordinated Hypothalamic and Reward Circuits. *Neuron* **103**, 891-908.e6 (2019).

16. Han, W. *et al.* A Neural Circuit for Gut-Induced Reward. *Cell* **175**, 665-678.e23 (2018).

885 17. Ferreira, J. G., Tellez, L. A., Ren, X., Yeckel, C. W. & de Araujo, I. E. Regulation of fat intake in the absence of flavour signalling. *J. Physiol.* **590**, 953–972 (2012).

18. Ren, X. *et al.* Nutrient Selection in the Absence of Taste Receptor Signaling. *J. Neurosci.* **30**, 8012–8023 (2010).

19. Han, W. *et al.* Striatal Dopamine Links Gastrointestinal Rerouting to Altered Sweet

890 Appetite. *Cell Metab.* **23**, 103–112 (2016).

20. Zhuo, Y. *et al.* Improved green and red GRAB sensors for monitoring dopaminergic activity in vivo. *Nat. Methods* **21**, 680–691 (2024).

21. Krettek, J. E. & Price, J. L. A description of the amygdaloid complex in the rat and cat with observations on intra-amygdaloid axonal connections. *J. Comp. Neurol.* **178**, 255–279

895 (1978).

22. Wang, L. *et al.* The coding of valence and identity in the mammalian taste system. *Nature* **558**, 127–131 (2018).

23. Hintiryan, H. *et al.* Connectivity characterization of the mouse basolateral amygdalar complex. *Nat. Commun.* **12**, 2859 (2021).

24. Lutas, A. *et al.* State-specific gating of salient cues by midbrain dopaminergic input to basal amygdala. *Nat. Neurosci.* **22**, 1820–1833 (2019).

25. Sclafani, A., Koepsell, H. & Ackroff, K. SGLT1 sugar transporter/sensor is required for post-oral glucose appetition. *Am. J. Physiol.-Regul. Integr. Comp. Physiol.* **310**, R631–R639 (2016).

26. Zukerman, S., Ackroff, K. & Sclafani, A. Post-oral appetite stimulation by sugars and nonmetabolizable sugar analogs. *Am. J. Physiol.-Regul. Integr. Comp. Physiol.* **305**, R840–R853 (2013).

27. Ackroff, K. & Sclafani, A. Post-oral fat stimulation of intake and conditioned flavor preference in C57BL/6J mice: A concentration-response study. *Physiol. Behav.* **129**, 64–72 (2014).

28. Sclafani, A., Zukerman, S. & Ackroff, K. GPR40 and GPR120 fatty acid sensors are critical for postoral but not oral mediation of fat preferences in the mouse. *Am. J. Physiol.-Regul. Integr. Comp. Physiol.* **305**, R1490–R1497 (2013).

29. Sclafani, A., Ackroff, K. & Abumrad, N. A. CD36 gene deletion reduces fat preference and intake but not post-oral fat conditioning in mice. *Am. J. Physiol.-Regul. Integr. Comp. Physiol.* **293**, R1823–R1832 (2007).

30. Fernandes, A. B. *et al.* Postingestive Modulation of Food Seeking Depends on Vagus-Mediated Dopamine Neuron Activity. *Neuron* **106**, 778-788.e6 (2020).

31. Poulin, J.-F. *et al.* Mapping projections of molecularly defined dopamine neuron subtypes using intersectional genetic approaches. *Nat. Neurosci.* **21**, 1260–1271 (2018).

32. Leshan, R. L. *et al.* Ventral Tegmental Area Leptin Receptor Neurons Specifically Project to and Regulate Cocaine- and Amphetamine-Regulated Transcript Neurons of the Extended Central Amygdala. *J. Neurosci.* **30**, 5713–5723 (2010).

33. Flagel, S. B. *et al.* A selective role for dopamine in stimulus–reward learning. *Nature* **469**, 53–57 (2011).

34. Saddoris, M. P., Cacciapaglia, F., Wightman, R. M. & Carelli, R. M. Differential Dopamine Release Dynamics in the Nucleus Accumbens Core and Shell Reveal Complementary Signals for Error Prediction and Incentive Motivation. *J. Neurosci.* **35**, 11572–11582 (2015).

35. Han, X. *et al.* Role of dopamine projections from ventral tegmental area to nucleus accumbens and medial prefrontal cortex in reinforcement behaviors assessed using optogenetic manipulation. *Metab. Brain Dis.* **32**, 1491–1502 (2017).

36. Sias, A. C. *et al.* Dopamine projections to the basolateral amygdala drive the encoding of identity-specific reward memories. *Nat. Neurosci.* **27**, 728–736 (2024).

37. Boekhoudt, L. *et al.* Does activation of midbrain dopamine neurons promote or reduce feeding? | International Journal of Obesity. *Int. J. Obes.* **41**, 1131–1140 (2017).

38. Wei, X. *et al.* Dopamine D1 or D2 receptor-expressing neurons in the central nervous system. *Addict. Biol.* **23**, 569–584 (2018).

39. Baas, D., Aleman, A. & Kahn, R. S. Lateralization of amygdala activation: a systematic review of functional neuroimaging studies. *Brain Res. Rev.* **45**, 96–103 (2004).

40. Baker, K. B. & Kim, J. J. Amygdalar Lateralization in Fear Conditioning: Evidence for Greater Involvement of the Right Amygdala. *Behav. Neurosci.* **118**, 15–23 (2004).

41. Allen, H. N., Bobnar, H. J. & Kolber, B. J. Left and right hemispheric lateralization of the amygdala in pain. *Prog. Neurobiol.* **196**, 101891 (2021).

42. Thanarajah, S. E. *et al.* Food Intake Recruits Orosensory and Post-ingestive Dopaminergic Circuits to Affect Eating Desire in Humans. *Cell Metab.* **29**, 695-706.e4 (2019).

43. de Araujo, A. M. *et al.* Asymmetric control of food intake by left and right vagal sensory neurons. *bioRxiv* 2023.05.08.539627 (2023) doi:10.1101/2023.05.08.539627.

44. Qian, K., Liu, J., Cao, Y., Yang, J. & Qiu, S. Intraperitoneal injection of lithium chloride induces lateralized activation of the insular cortex in adult mice. *Mol. Brain* **14**, 71 (2021).

45. Wu, Y. *et al.* The anterior insular cortex unilaterally controls feeding in response to aversive visceral stimuli in mice. *Nat. Commun.* **11**, 640 (2020).

46. Breton, J. M. *et al.* Relative Contributions and Mapping of Ventral Tegmental Area Dopamine and GABA Neurons by Projection Target in the Rat. *J. Comp. Neurol.* **527**, 916–941 (2019).

47. Yates, S. C. *et al.* Frontiers | QUINT: Workflow for Quantification and Spatial Analysis of Features in Histological Images From Rodent Brain. https://doi.org/10.3389/fninf.2019.00075 doi:10.3389/fninf.2019.00075.

48. Wang, Q. *et al.* The Allen Mouse Brain Common Coordinate Framework: A 3D Reference Atlas. *Cell* **181**, 936-953.e20 (2020).

49. Matsumura, S. *et al.* Intragastric infusion of glucose enhances the rewarding effect of sorbitol fatty acid ester ingestion as measured by conditioned place preference in mice. *Physiol. Behav.* **99**, 509–514 (2010).

50. de Araujo, I. E., Schatzker, M. & Small, D. M. Rethinking food reward. *Annu. Rev. Psychol.* **71**, 139–164 (2020).

51. Tellez, L. A. *et al.* Separate circuitries encode the hedonic and nutritional values of sugar. *Nat. Neurosci.* **19**, 465–470 (2016).

52. Zhang, L., Han, W., Lin, C., Li, F. & Araujo, I. E. de. Sugar Metabolism Regulates Flavor Preferences and Portal Glucose Sensing. *Front. Integr. Neurosci.* **12**, (2018).

53. de Araujo, I. E. Circuit organization of sugar reinforcement. *Physiol. Behav.* **164**, 473–477 (2016).

54. McCutcheon, J. E. The role of dopamine in the pursuit of nutritional value. *Physiol. Behav.* **152**, 408–415 (2015).

55. McDougle, M. *et al.* Separate gut-brain circuits for fat and sugar reinforcement combine to promote overeating. *Cell Metab.* **36**, 393-407.e7 (2024).

56. Krabbe, S., Gründemann, J. & Lüthi, A. Amygdala Inhibitory Circuits Regulate Associative Fear Conditioning. https://www.biologicalpsychiatryjournal.com/article/S0006-3223(17)32062-0/fulltext.

57. Wassum, K. M. & Izquierdo, A. The basolateral amygdala in reward learning and addiction. *Neurosci. Biobehav. Rev.* **57**, 271–283 (2015).

58. Cartoni, E., Balleine, B. & Baldassarre, G. Appetitive Pavlovian-instrumental Transfer: A review. *Neurosci. Biobehav. Rev.* **71**, 829–848 (2016).

59. Izhikevich, E. M. Solving the Distal Reward Problem through Linkage of STDP and Dopamine Signaling. *Cereb. Cortex* **17**, 2443–2452 (2007).

60. Yagishita, S. *et al.* A critical time window for dopamine actions on the structural plasticity of dendritic spines. *Science* **345**, 1616–1620 (2014).

61. Ghika-Schmid, F., Assal, G., De Tribolet, N. & Regli, F. Klüver-Bucy syndrome after left anterior temporal resection. *Neuropsychologia* **33**, 101–113 (1995).

62. Anson, J. A. & Kuhlman, D. T. Post-ictal Kluver-Bucy syndrome after temporal lobectomy. *J. Neurol. Neurosurg. Psychiatry* **56**, 311–313 (1993).

63. Boronat, S., Newberry, P., Mehan, W., Thiele, E. A. & Duhaime, A.-C. Klüver–Bucy syndrome after unilateral frontotemporal resection in a child with tuberous sclerosis. *Childs Nerv. Syst.* **29**, 1391–1394 (2013).

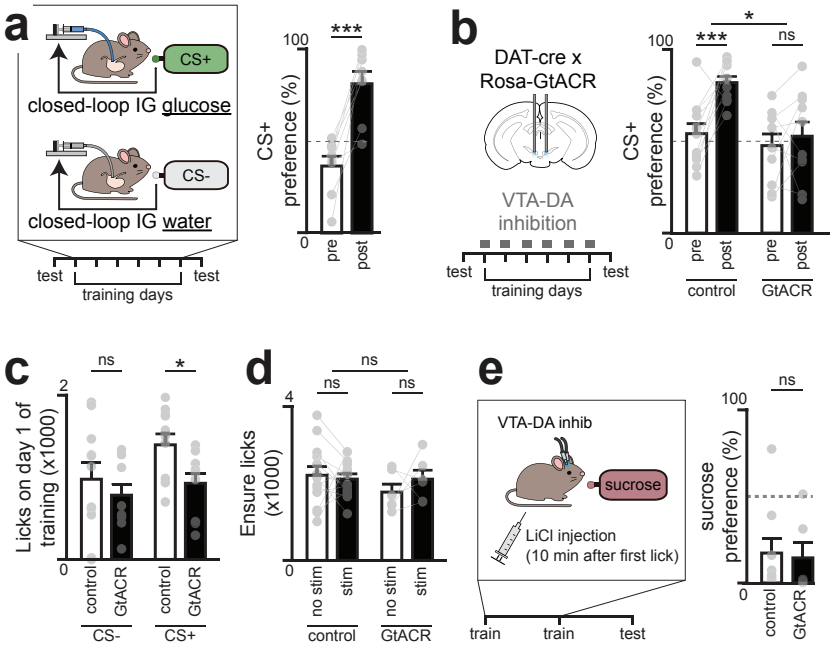

Figure 1. Dopamine neurons are necessary for nutrient learning.
a, Flavor–nutrient conditioning protocol (left); mice learned to prefer the glucose-paired flavor (CS+, right).
b, Inhibition of VTA-DA neurons during conditioning (left) prevented flavor–nutrient learning (right).
c, VTA-DA inhibition reduced CS+ intake on the first training day.
d, Inhibition did not reduce intake of the familiar nutritive solution Ensure.
e, Flavor avoidance conditioning protocol (left); VTA-DA inhibition did not prevent acquisition of conditioned flavor avoidance (right).
ns $P > 0.05$; *$P < 0.05$; **$P < 0.01$; ***$P < 0.001$. See Extended Data Table 1.

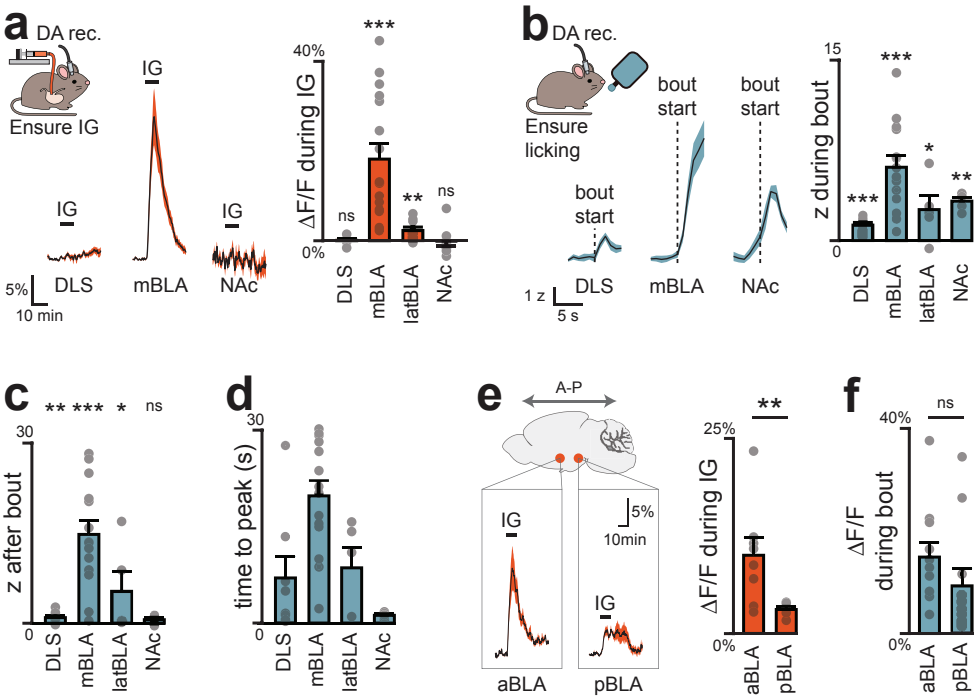

Figure 2. Distinct dopamine pathway tracks internal nutrients.
a, Dopamine release recorded with the fluorescent sensor GRAB-DA during Ensure IG infusion, showing responses localized to BLA.
b, Dopamine release 5 s into the first lick bout, showing distributed responses.
c, Dopamine release 5 s after the first lick bout, showing sustained activity in BLA.
d, Peak times within 30 s of the first lick bout. Note prolonged BLA responses.
e, During IG infusion, dopamine release was greatest in anterior BLA (aBLA).
f, During the first lick bout, dopamine release was similar across BLA subregions.
ns $P > 0.05$; *$P < 0.05$; **$P < 0.01$; ***$P < 0.001$. See Extended Data Table 2.

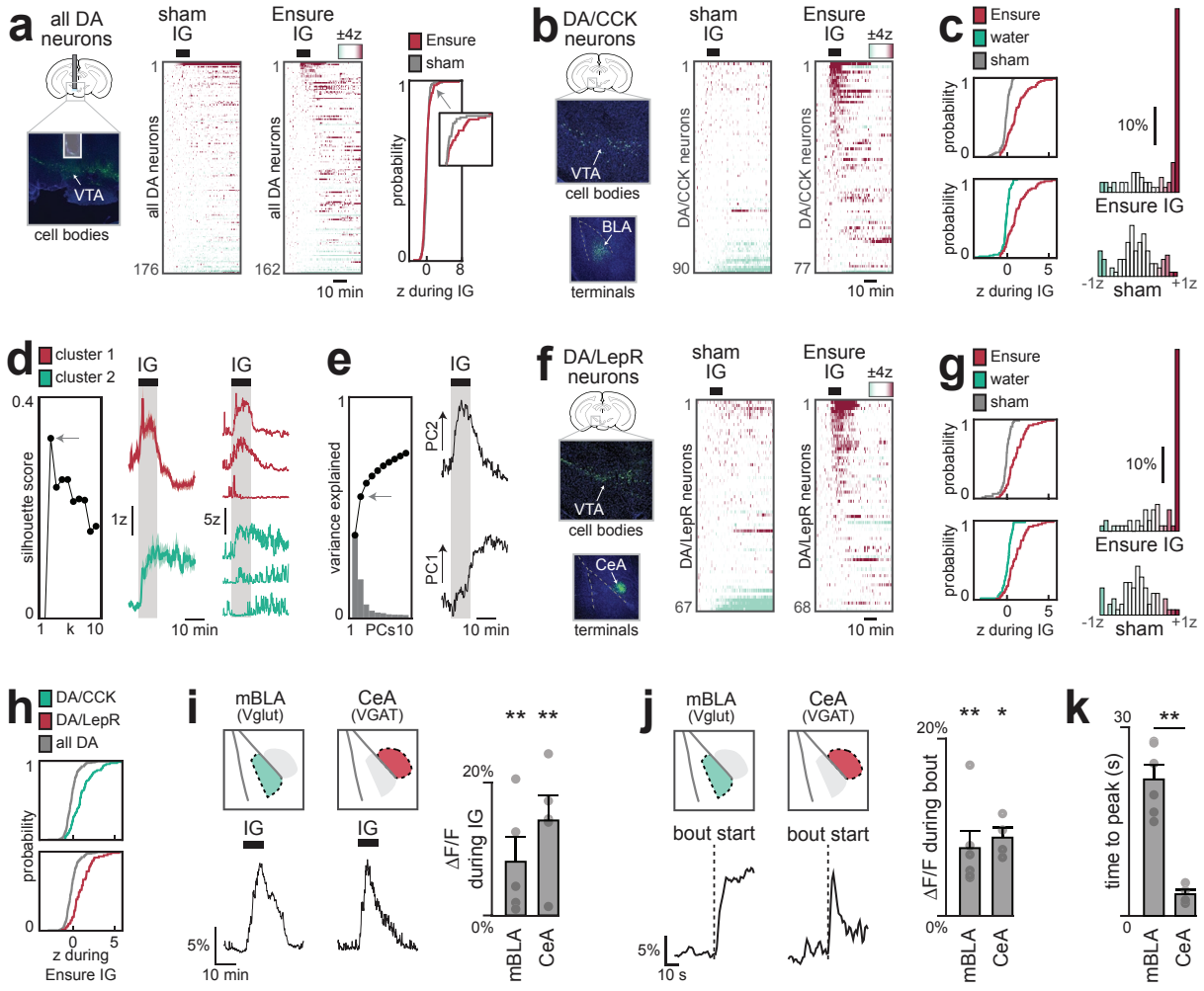

Figure 3. Genetically defined VTA dopamine projections track nutrient ingestion.
a, Single-cell dynamics of VTA-DA neurons during Ensure or sham infusion. A small subpopulation showed greater activation during Ensure infusion vs sham (p = 0.018).
b–e, VTA-DA/CCK neurons (cell bodies in VTA, terminals in BLA). b, Single-cell dynamics during Ensure or sham infusion. c, Cumulative distributions and binned activity show increased responses during Ensure IG vs sham (p = 2.0e-13) or water (p = 8.8e-13). d, K-means clustering reveals transient (magenta) and prolonged (mint) subpopulations, shown with mean and representative single-neuron activity. e, Principal component analysis; the first two PCs explain 55% of variance and correspond to activity changes during and after infusion.
f–h, VTA-DA/LepR neurons (cell bodies in VTA, terminals in CeA). f, Single-cell dynamics during Ensure or sham infusion. Note lack of sustained Ensure response, relative to CCK subpopulation. g, Cumulative distributions and binned activity show increased responses during Ensure IG vs sham (p = 6.8e-10) or water (p = 4.9e-7). h, Cumulative distributions show increased activation across both CCK and LepR subpopulations (CCK, p = 4.2e-11; LepR, p = 2.3e-12).
i–k, Fiber photometry recordings of DA release in BLA and CeA using region-specific Cre drivers (Vglut-cre, VGAT-cre). i, Dopamine increased in both regions during
Ensure IG (left: example traces; right: summary plots). j, Dopamine increased in both regions 5s into the first Ensure lick bout (left: example traces; right: summary plots).
k, Lick-triggered DA release peaks earlier in CeA.
*P < 0.05; **P < 0.01; ***P < 0.001. See Extended Data Tables 2, 3.

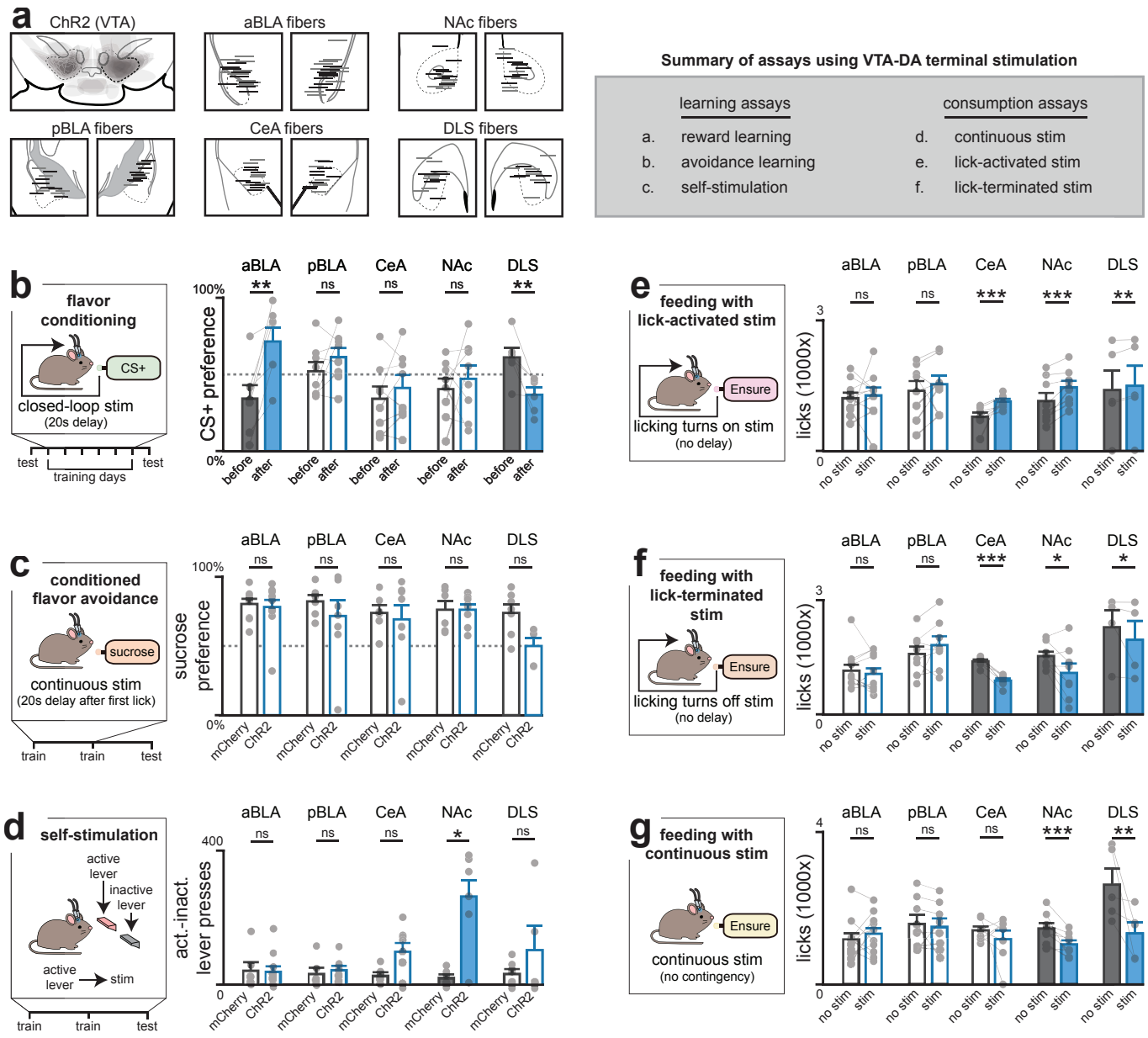

Figure 4. Distinct roles of BLA dopamine projections in feeding and flavor learning.
a, (Top) Viral expression of ChR2 in VTA-DA neurons and fiber placement above projection targets (grey=mCherry, black=ChR2, left) and summary of assays (right).
b, Flavor conditioning assay (during training, each lick triggered stimulation after a 20s delay, replicating IG transit time).
c, Conditioned flavor avoidance assay (during training, continuous stimulation was given after the first lick with a 20s delay).
d, Self-stimulation assay (during training, the active lever provided stimulation with no delay).
e, Consumption during lick-activated stimulation (no delay).
f, Consumption during lick-terminated stimulation (no delay).
g, Consumption during continuous stimulation (no contingency).
ns $P > 0.05$; *$P < 0.05$; **$P < 0.01$; ***$P < 0.001$, after Benjamini–Hochberg correction (see Extended Data Table 1).

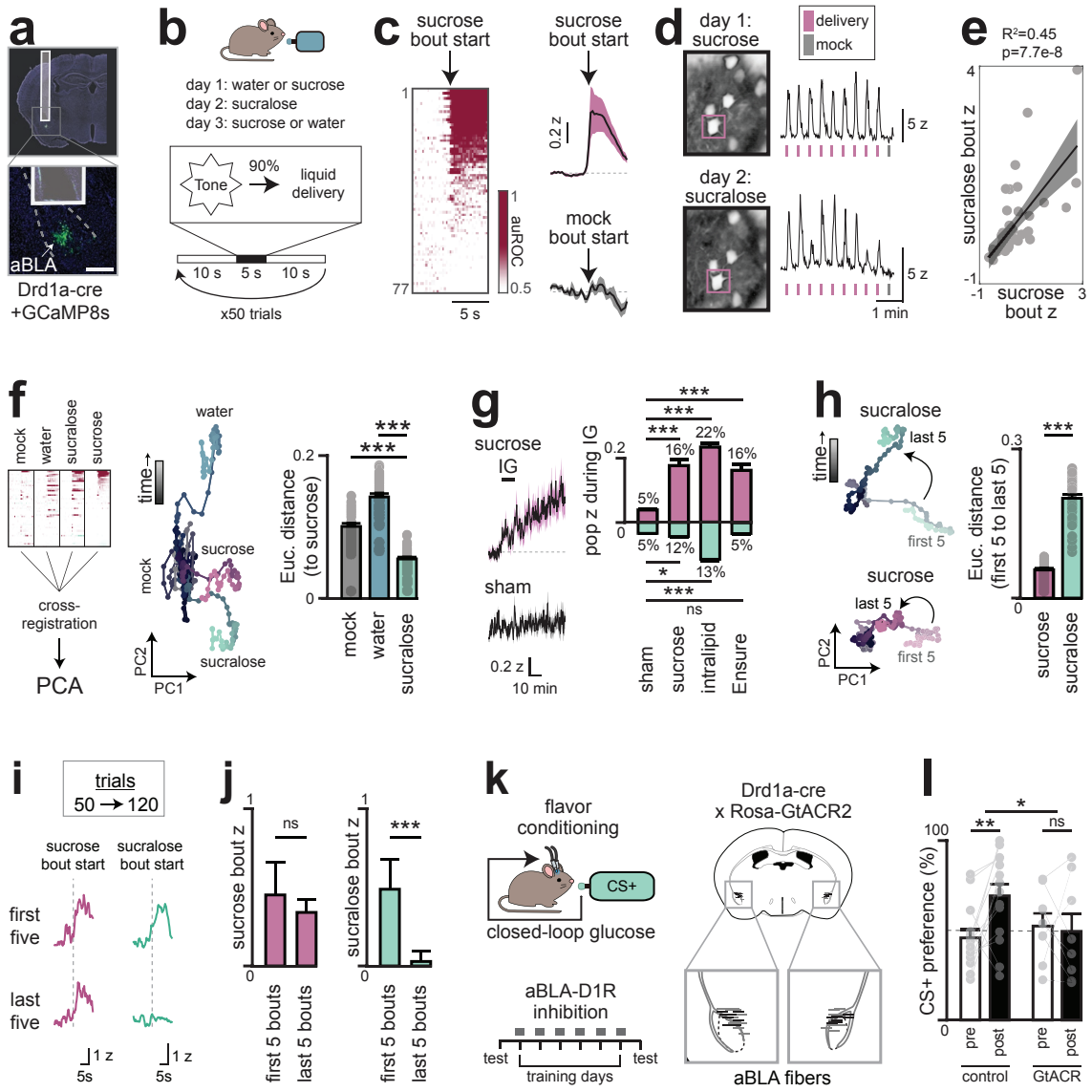

Figure 5. aBLA neurons integrate oral and post-ingestive nutrient signals.
a, Imaging of D1R-expressing aBLA neurons (scale bar, 0.5 mm).
b, Protocol for recording taste responses.
c, Single-cell dynamics during sucrose delivery, quantified by auROC (left), and mean activity across sucrose vs no-delivery bouts (right).
d–e, Cross-registered neurons across days. d, Example FOVs and activity of a single neuron during sucrose (day 1) and sucralose (day 2) delivery. e, Correlation of activity during sucrose vs sucralose bouts.
f, PCA of cross-registered neurons across three days shows similar activity trajectories for sucrose and sucralose, quantified by euclidian distance across PC1–2 for each timepoint.
g, Mean activity traces during IG infusions (left), and population-weighted z-scores of activated (magenta) and inhibited (mint) neurons (right).
h, Lick-triggered activity diverged across early and late sucralose (but not sucrose) bouts, shown in PC space (left) and by Euclidean distance across PC1–2 (right).
i–j, Increasing trials to 120 reveals further changes in responsivity. i, Activity of one neuron during early and late sucrose (left) and sucralose (right) bouts. j, Sucralose (but not sucrose) responses decayed over time.
k–l, Inhibition of aBLA-D1R neurons during flavor–nutrient conditioning. k, Protocol (left) and fiber placement (right; grey=littermate controls, black=GtACR). l, Silencing prevented conditioned flavor preference.
ns P > 0.05; *P < 0.05; **P < 0.01; ***P < 0.001. See Extended Data Tables 1, 3.

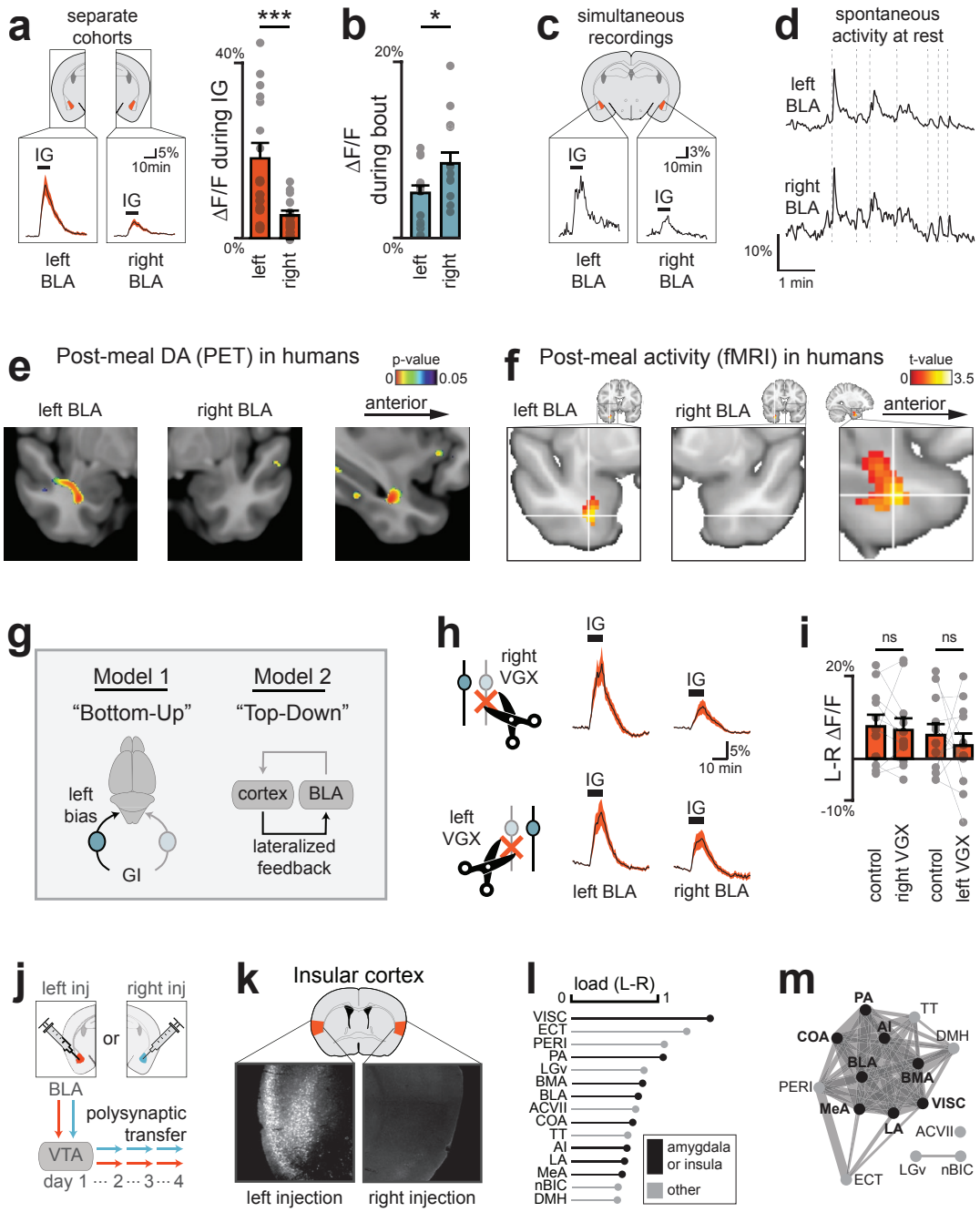

Figure 6. Lateralized DA pathway tracks internal nutrients.
a–b, Unilateral recordings in left or right BLA. a. Mean DA release during Ensure IG infusion is greater in left BLA (left, mean traces; right, summary plots). b, DA release during the first lick bout is greater in right BLA.
c–d, Simultaneous recordings in left and right BLA. c. Example from one mouse showing DA activity in left and right BLA during Ensure IG infusion. d, Example a
e, In humans, PET imaging (11C-raclopride) shows left-lateralized DA release after milkshake, strongest in anterior BLA.
f, fMRI shows greater left BLA activation after glucose vs water consumption.
g, Left dominance may arise from (1) asymmetric vagal input, or (2) lateralized feedback circuitry.
h, Bilateral BLA dopamine recordings after unilateral vagotomy (VGX).
i, Neither left nor right vagotomy abolishes lateralization.
j, Polysynaptic retrograde tracing mapped inputs to left vs right VTA→BLA dopamine pathways.
k, Left pathway receives stronger input from insular cortex.
l, Top fifteen regions showing greater labeling after left vs right BLA injection (normalized to VTA labeling; n = 8 left injections, 6 right injections).
m, Force-directed graph illustrating strong connectivity among regions in (l).
Brains shown in neurological orientation (left = subject's left). Full list of abbreviations in Ex. Fig. 16.
ns P > 0.05; *P < 0.05; **P < 0.01; ***P < 0.001. See Extended Data Tables 2, 4.

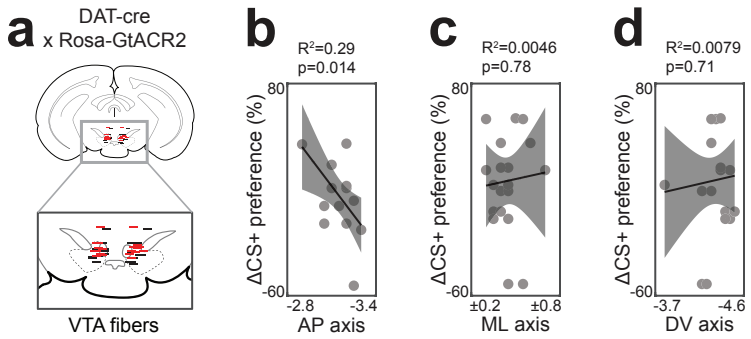

Extended Data Fig. 1. Fiber localization for VTA-DA inhibition experiments.
a, Fiber placement in VTA, shown with median slice along anteroposterior (AP) axis (black=littermate controls, red=GtACR).
b, Mice with fibers above posterior VTA showed greater inhibition of flavor learning, consistent with the location of the BLA projecting population (Lammel et al., 2008).
c, Fiber placement along the mediolateral (ML) axis did not affect learning, as deviations would cancel within animals due to the fixed bilateral spacing of implants.
d, Fiber placement along the dorsoventral (DV) axis did not affect learning.
ns $P > 0.05$; *$P < 0.05$; **$P < 0.01$; ***$P < 0.001$. See Extended Data Table 1.

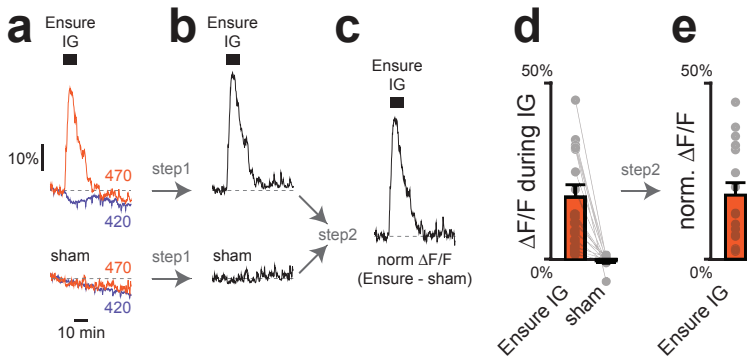

Extended Data Figure 2. Dopamine signal normalization for long recordings.
Two-step normalization procedure. Step 1: fluorescence traces normalized to activity-independent signal (420 nm), removing movement artefacts. Step 2: traces during IG or IP manipulations further normalized to sham infusion or saline injection, correcting for bleaching and long-term drift. Outside this figure, only step 1 normalization was applied to activity traces, and step 2 was applied only to summary plots.
a, Example raw fluorescence traces from a single mBLA GRAB-DA site during Ensure IG (top) or sham (bottom).
b, Dopamine-dependent signal after 470 nm traces were normalized to 420 nm.
c, Further normalization by subtracting sham traces.
d, Summary of mBLA dopamine release during Ensure IG vs sham after step 1.
e, Summary of the same data after both steps.

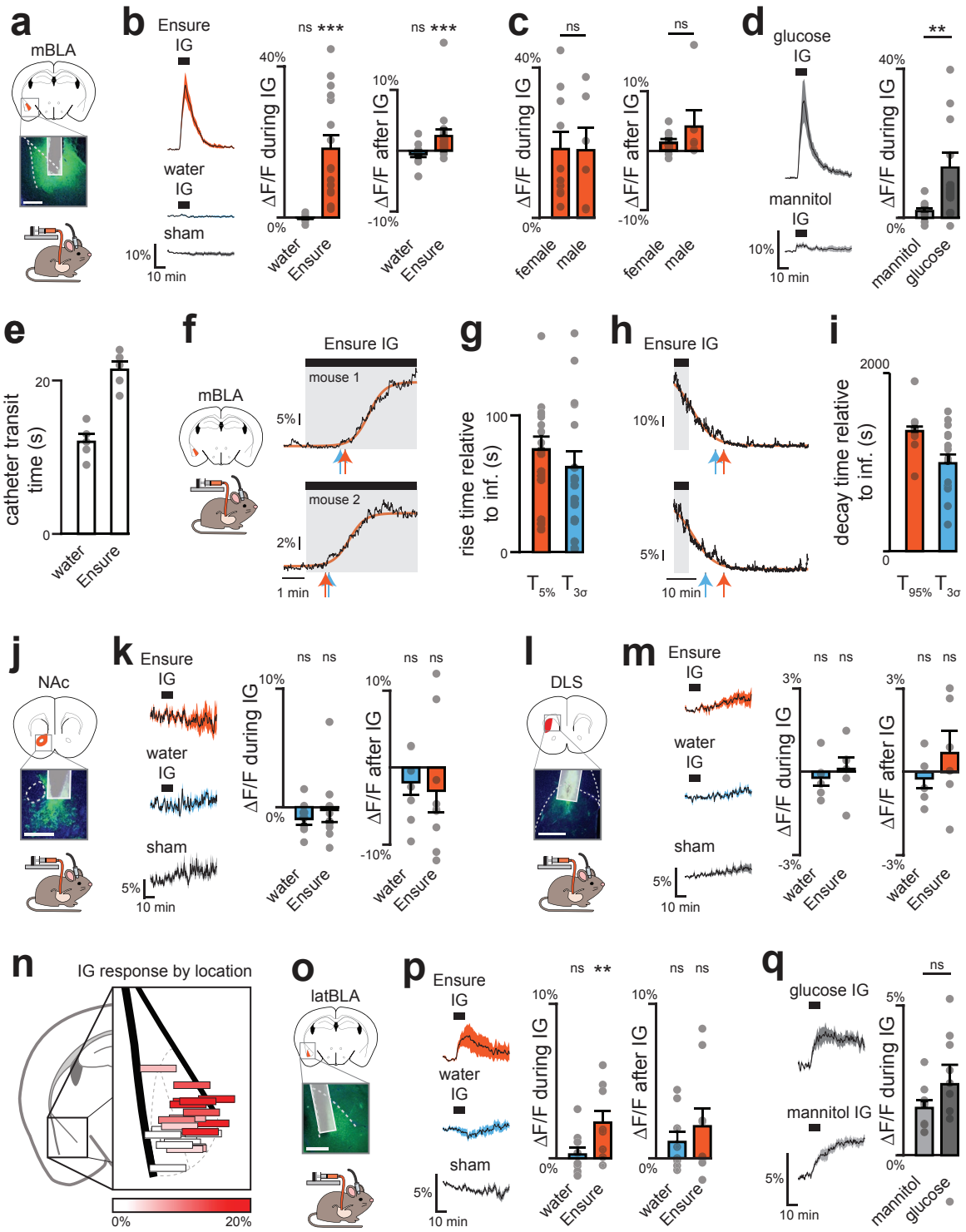
a
mBLA
b
Ensure IG
water IG
sham
10%
10 min
ns ***
ΔF/F during IG
40%
0%
water
Ensure
ns ***
ΔF/F after IG
10%
-10%
c
ns
ΔF/F during IG
40%
0%
female
male
ns
ΔF/F after IG
10%
-10%
d
glucose IG
mannitol IG
10%
10 min
**
ΔF/F during IG
40%
0%
mannitol
glucose
e
catheter transit time (s)
20
0
water
Ensure
f
mBLA
Ensure IG
mouse 1
5%
mouse 2
2%
1 min
g
rise time relative to inf. (s)
100
0
T5%
T3σ
h
Ensure IG
10%
5%
10 min
i
decay time relative to inf. (s)
2000
0
T95%
T3σ
j
NAc
k
Ensure IG
water IG
sham
5%
10 min
ns ns
ΔF/F during IG
10%
0%
water
Ensure
ns ns
ΔF/F after IG
10%
-10%
l
DLS
m
Ensure IG
water IG
sham
5%
10 min
ns ns
ΔF/F during IG
3%
-3%
water
Ensure
ns ns
ΔF/F after IG
3%
-3%
n
IG response by location
0%
20%
o
latBLA
p
Ensure IG
water IG
sham
5%
10 min
ns **
ΔF/F during IG
10%
0%
water
Ensure
ns ns
ΔF/F after IG
10%
0%
water
Ensure
q
glucose IG
mannitol IG
5%
10 min
ns
ΔF/F during IG
5%
0%
mannitol
glucose

Extended Data Figure 3. Dopamine dynamics across brain regions during IG infusions.
a, GRAB-DA recordings in mBLA; dotted lines mark external capsule (scale bar, 0.5 mm).
b, Mean traces (left) and summary plots (middle, right) showing greater mBLA DA release during and after Ensure infusion.
c, No sex differences in mBLA DA release during (left) or after (right) Ensure infusion.
d, Glucose, but not mannitol, increases mBLA DA release.
e, Transit times for IG infusions: water 12 ± 1 s; Ensure 21 ± 1 s.
f, Example traces with sigmoid fits to estimate T5% (orange) and T3σ (blue).
g, Summary rise times relative to infusion onset, corrected for transit time (from e): T5% = 54 ± 9 s; T3σ = 41 ± 12 s; mean = 48 ± 11 s.
h, Example traces with sigmoid fits to estimate T95% (orange) and T3σ (blue).
i, Summary decay times relative to infusion end: T95% = 749 ± 51 s; T3σ = 388 ± 100 s; mean = 569 ± 79 s.
j, GRAB-DA recordings in NAc core; dotted lines mark anterior commissure (scale bar, 0.5 mm).
k, No change in NAc DA release with Ensure or water.
l, GRAB-DA recordings in DLS; dotted lines mark corpus callosum (scale bar, 0.5 mm).
m, No change in DLS DA release with Ensure or water.
n, Reconstructed fiber placements in BLA (color scale = $\Delta F/F$ during Ensure IG), showing greater DA release in magnocellular vs parvocellular BLA.
o, GRAB-DA recordings in lateral BLA; dotted lines mark external capsule (scale bar, 0.5 mm).
p, Lateral BLA shows increased DA release during Ensure infusion, but not after.
q, Both glucose and mannitol increase DA release in lateral BLA.
ns $P > 0.05$; *$P < 0.05$; **$P < 0.01$; ***$P < 0.001$. See Extended Data Table 2.

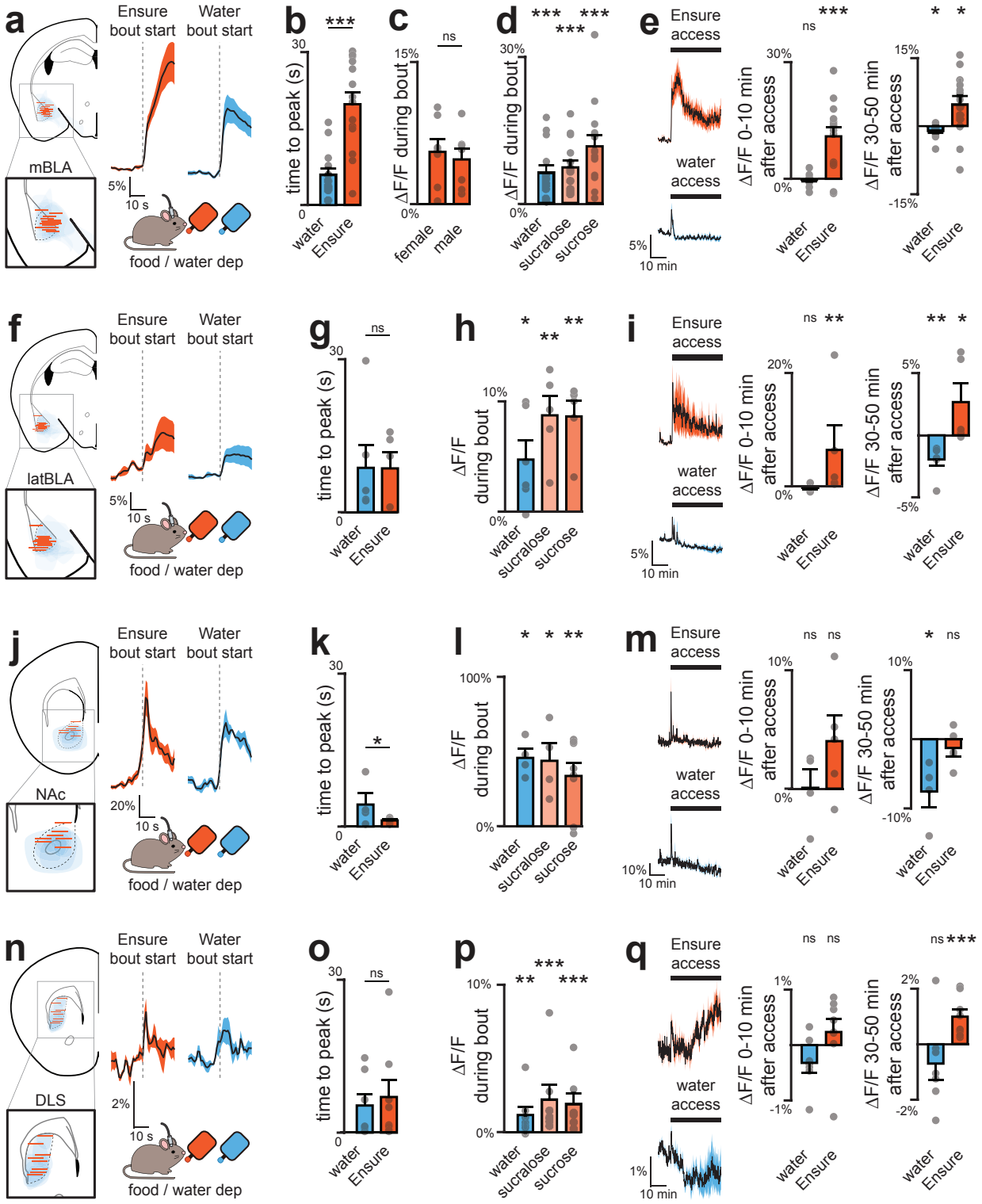
a
Ensure bout start
Water bout start
mBLA
5%
10 s
food / water dep
b
***
time to peak (s)
30
0
water
Ensure
c
ns
ΔF/F during bout
15%
0%
female
male
d
***
***
***
ΔF/F during bout
30%
0%
water
sucralose
sucrose
e
Ensure access
water access
5%
10 min
ns
***
ΔF/F 0-10 min after access
30%
0%
water
Ensure
*
*
ΔF/F 30-50 min after access
15%
-15%
water
Ensure
f
Ensure bout start
Water bout start
latBLA
5%
10 s
food / water dep
g
ns
time to peak (s)
30
0
water
Ensure
h
*
**
**
ΔF/F during bout
10%
0%
water
sucralose
sucrose
i
Ensure access
water access
5%
10 min
ns
**
ΔF/F 0-10 min after access
20%
0%
water
Ensure
**
*
ΔF/F 30-50 min after access
5%
-5%
water
Ensure
j
Ensure bout start
Water bout start
NAc
20%
10 s
food / water dep
k
*
time to peak (s)
30
0
water
Ensure
l
*
*
**
ΔF/F during bout
100%
0%
water
sucralose
sucrose
m
Ensure access
water access
10%
10 min
ns
ns
ΔF/F 0-10 min after access
10%
0%
water
Ensure
*
ns
ΔF/F 30-50 min after access
10%
-10%
water
Ensure
n
Ensure bout start
Water bout start
DLS
2%
10 s
food / water dep
o
ns
time to peak (s)
30
0
water
Ensure
p
***
**
***
ΔF/F during bout
10%
0%
water
sucralose
sucrose
q
Ensure access
water access
1%
10 min
ns
ns
ΔF/F 0-10 min after access
1%
-1%
water
Ensure
ns
***
ΔF/F 30-50 min after access
2%
-2%
water
Ensure

Extended Data Figure 4. Dopamine dynamics across brain regions during natural consumption.
a, Fiber placement and viral spread for mBLA recordings (left). Mean GRAB-DA responses during first lick bout of Ensure following food deprivation (middle) and water following water deprivation (right).`
b, mBLA DA peak time is delayed following Ensure vs water.
c, No sex differences in mBLA DA release during first Ensure lick bout.
d, Summary plots of mBLA DA release during first lick bouts.
e, Mean traces (left) and summary plots (middle, right) showing long-term mBLA DA increases during Ensure consumption.
f, Fiber placement and viral spread for lateral BLA recordings (left). Mean GRAB-DA responses during first lick bout of Ensure and water (middle, right).
g, Peak time of lateral BLA DA release.
h, Summary plots of lateral BLA DA release during first lick bouts.
i, Mean traces (left) and summary plots (middle, right) showing long-term lateral BLA DA increases during Ensure consumption.
j, Fiber placement and viral spread for NAc recordings (left). Mean GRAB-DA responses during first lick bout of Ensure and water (middle, right).
k, Peak time of NAc DA release.
l, Summary plots of NAc DA release during first lick bouts.
m, Mean traces (left) and summary plots (middle, right) showing no long-term NAc DA increase during Ensure consumption.
n, Fiber placement and viral spread for DLS recordings (left). Mean GRAB-DA responses during first lick bout of Ensure and water (middle, right).
o, Peak time of DLS DA release.
p, Summary plots of DLS DA release during first lick bouts.
q, Traces (left) and summary plots (middle, right) showing long-term DLS DA increases during Ensure consumption.
ns $P > 0.05$; *$P < 0.05$; **$P < 0.01$; ***$P < 0.001$. See Extended Data Table 2.

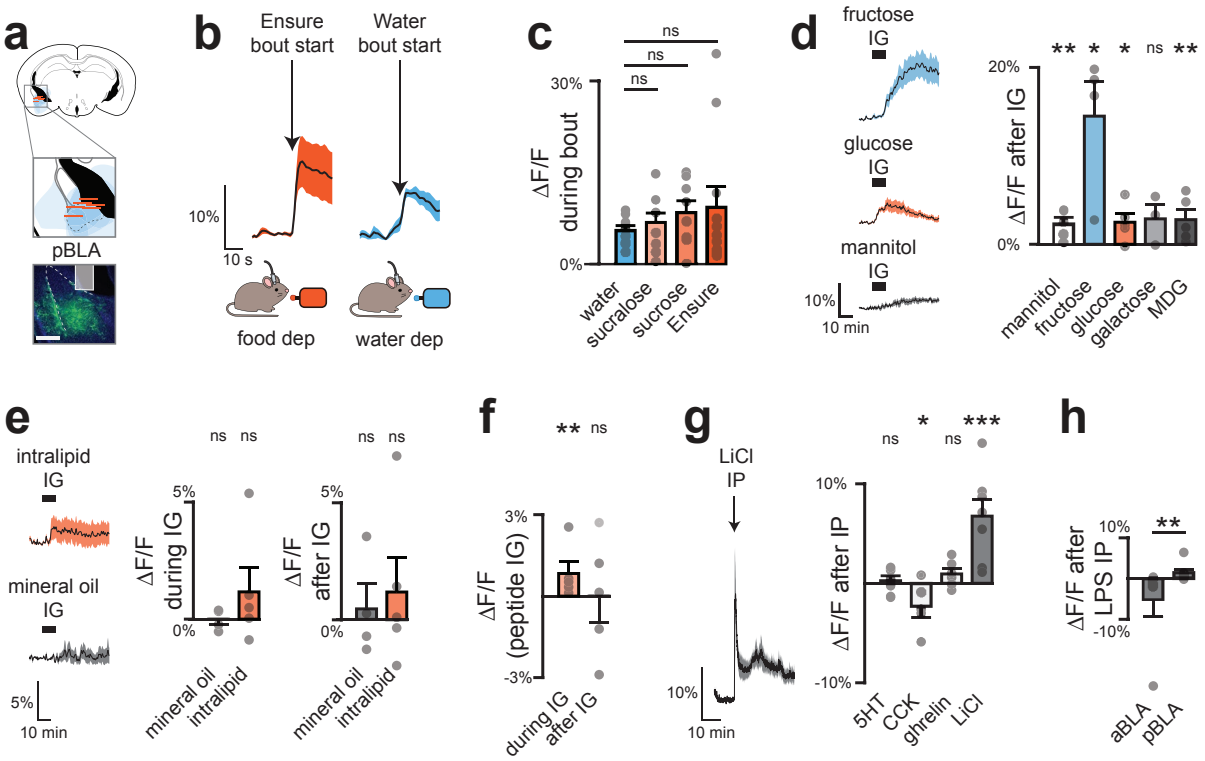

Extended Data Fig. 5 | Dopamine release in posterior BLA (pBLA) does not depend on nutrients.
a, Fiber placement and viral spread for pBLA recordings (scale bar, 0.5 mm).
b, DA dynamics during first lick bout of water and Ensure.
c, No difference in DA release during bouts of water vs nutrients.
d, Traces (left) and summary plots (right) showing increased DA release after IG sugar infusion, independent of SGLT1.
e, Traces (left) and summary plots (right) showing no DA increase after nutritive or non-nutritive fat infusions.
f, Small but significant DA release during peptide infusion.
g, Traces (left) and summary plots (right) showing no DA response to feeding hormones, but significant release to aversive LiCl (IP).
h, Increased pBLA DA and decreased aBLA DA following aversive LPS injection.
ns $P > 0.05$; *$P < 0.05$; **$P < 0.01$; ***$P < 0.001$. See Extended Data Table 2.

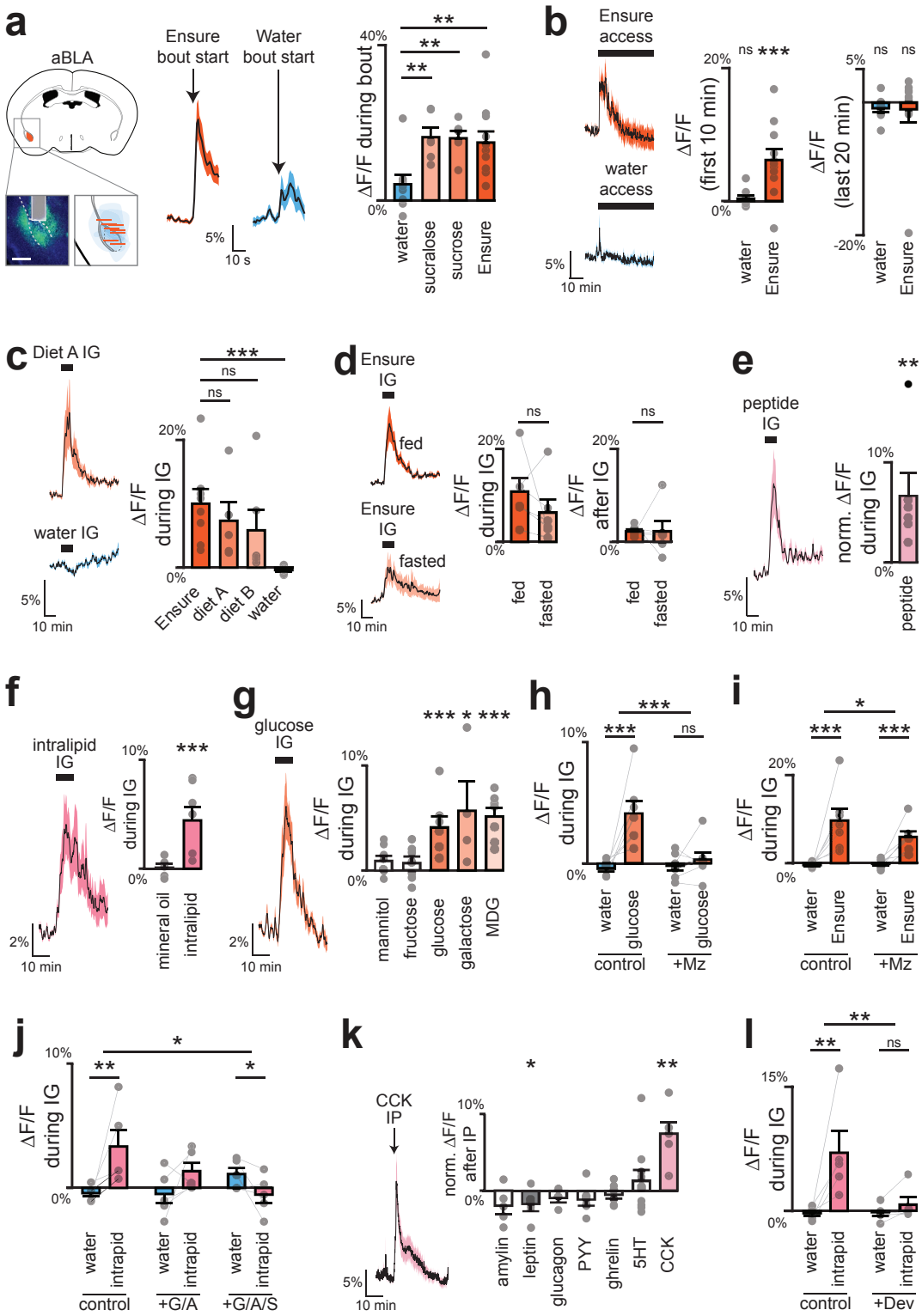
a
aBLA
Ensure bout start
Water bout start
5%
10 s
ΔF/F during bout
40%
0%
water
sucralose
sucrose
Ensure
b
Ensure access
water access
5%
10 min
ΔF/F (first 10 min)
20%
0%
ns
***
water
Ensure
ΔF/F (last 20 min)
5%
-20%
ns
ns
water
Ensure
c
Diet A IG
water IG
5%
10 min
ΔF/F during IG
20%
0%
***
ns
ns
Ensure
diet A
diet B
water
d
Ensure IG
fed
Ensure IG
fasted
5%
10 min
ΔF/F during IG
20%
0%
ns
fed
fasted
ΔF/F after IG
20%
0%
ns
fed
fasted
e
peptide IG
5%
10 min
norm. ΔF/F during IG
10%
0%
**
peptide
f
intralipid IG
2%
10 min
ΔF/F during IG
10%
0%
***
mineral oil
intralipid
g
glucose IG
2%
10 min
ΔF/F during IG
10%
0%
*** * ***
mannitol
fructose
glucose
galactose
MDG
h
ΔF/F during IG
10%
0%
***
***
ns
water
glucose
water
glucose
control
+Mz
i
ΔF/F during IG
20%
0%
*
***
***
water
Ensure
water
Ensure
control
+Mz
j
ΔF/F during IG
10%
0%
*
**
*
water
intrapid
water
intrapid
water
intrapid
control
+G/A
+G/A/S
k
CCK IP
5%
10 min
norm. ΔF/F after IP
10%
0%
*
**
amylin
leptin
glucagon
PYY
ghrelin
5HT
CCK
l
ΔF/F during IG
15%
0%
**
**
ns
water
intrapid
water
intrapid
control
+Dev

Extended Data Figure 6. Specific nutrients drive aBLA dopamine release.

a, Fiber placement and viral spread for aBLA recordings (left; scale bar, 0.5 mm). DA dynamics during first lick bout of water and Ensure (middle) with summary plot showing greater release to sweet solutions vs water (right).

b, Traces (left) and summary plots (right) of DA release during Ensure or water access.

c, Traces (left) and summary plots (right) during access to calorie-matched diets: diet A (55%/14%/31% sugar/-fat/protein, matches Ensure) and diet B (20%/20%/60%, matches mouse preference).

d, Traces (left) and summary plots (right) showing no difference in DA response to Ensure IG in fed vs fasted mice.

e, Traces (left) and summary plots (right) of DA release during peptide IG.

f, Traces (left) and summary plots (right) of DA release during intralipid vs mineral oil IG.

g, Traces (left) and summary plots (right) of DA responses to glucose and sugar analogs during IG.

h, Summary plot of DA responses during water or glucose IG with or without SGLT1 antagonist mizagliflozin (Mz).

i, Summary plot of DA responses during water or Ensure IG with or without mizagliflozin.

j, Summary plot of DA responses during water or intralipid IG with or without antagonists of GPR40 (GW1100, G), GPR120 (AH7614, A), or CD36 (sulfosuccinimidyl oleate, S).

k, Traces (left) and summary plots (right) of DA release during IP injection of CCK and other hormones.

l, Summary plot of DA release during water or intralipid IG with or without prior CCK antagonist devazepide (Dev).

ns $P > 0.05$; *$P < 0.05$; **$P < 0.01$; ***$P < 0.001$. See Extended Data Table 2.

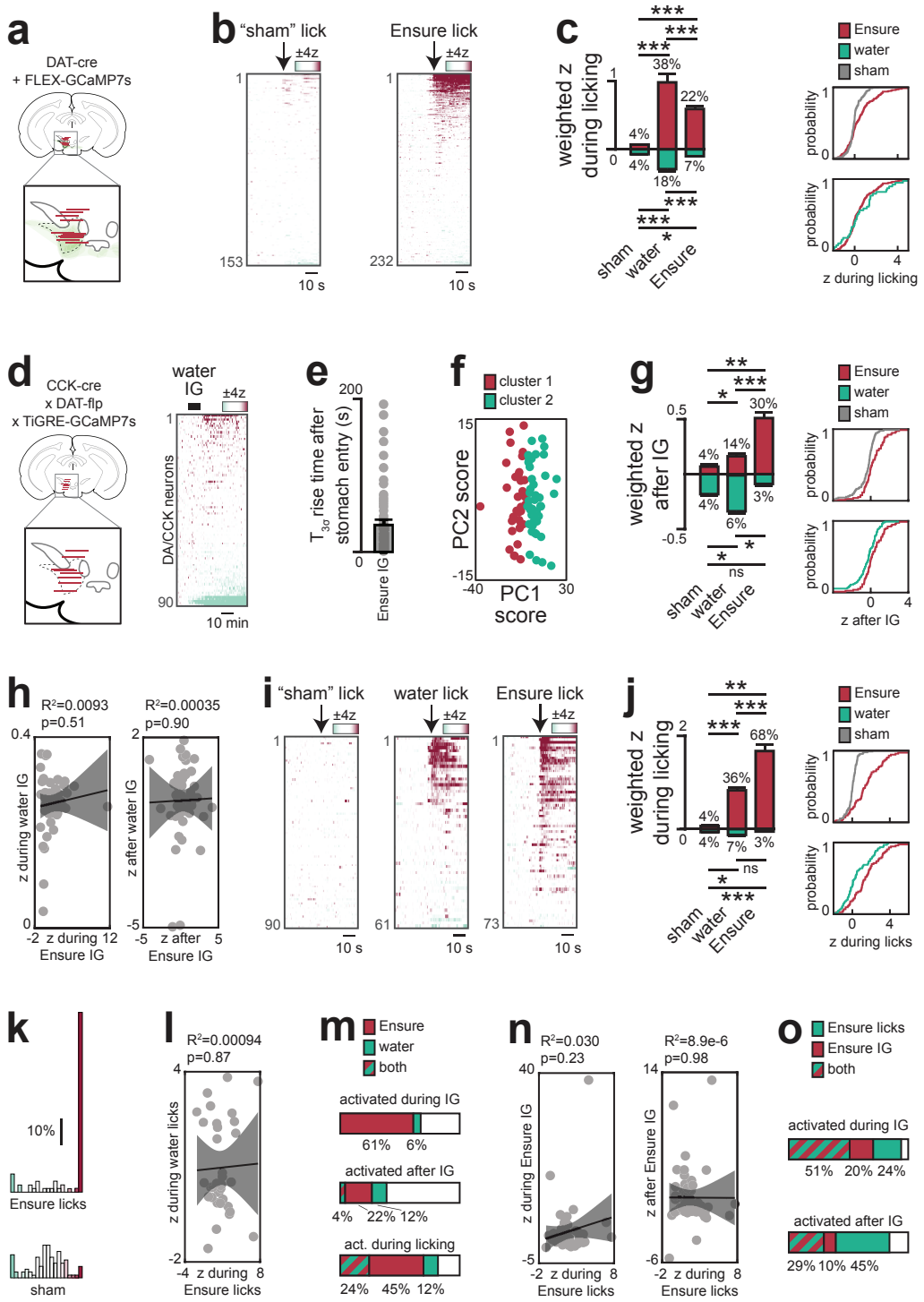
a
DAT-cre
+ FLEX-GCaMP7s
b
"sham" lick
Ensure lick
±4z
1
153
232
10 s
c
weighted z during licking
38%
22%
4%
4%
18%
7%
***
*
sham
water
Ensure
Ensure
water
sham
probability
z during licking
d
CCK-cre
x DAT-flp
x TiGRE-GCaMP7s
water IG
DA/CCK neurons
90
10 min
e
$T_{3\sigma}$ rise time after stomach entry (s)
200
0
Ensure IG
f
cluster 1
cluster 2
PC2 score
PC1 score
15
-15
-40
30
g
weighted z after IG
0.5
-0.5
30%
14%
4%
4%
6%
3%
**
***
*
ns
z after IG
h
R²=0.0093
p=0.51
R²=0.00035
p=0.90
z during water IG
z after water IG
z during Ensure IG
z after Ensure IG
i
"sham" lick
water lick
Ensure lick
90
61
73
j
weighted z during licking
68%
36%
4%
7%
3%
z during licks
k
10%
Ensure licks
sham
l
R²=0.00094
p=0.87
z during water licks
z during Ensure licks
m
Ensure
water
both
activated during IG
61% 6%
activated after IG
4% 22% 12%
act. during licking
24% 45% 12%
n
R²=0.030
p=0.23
R²=8.9e-6
p=0.98
z during Ensure IG
z after Ensure IG
z during Ensure licks
o
Ensure licks
Ensure IG
both
activated during IG
51% 20% 24%
activated after IG
29% 10% 45%

Extended Figure 7. DA/CCK subpopulation responses across different stages of ingestion.
a–c, Single-cell imaging of all VTA-DA neurons. a, Fiber placement and viral spread (left). b, Dynamics during consumption of Ensure or sham (see Methods).
c, Population-weighted activity of activated (magenta) and inhibited (mint) neurons (left) and cumulative distributions (right) showing increased activity during the first
Ensure bout (vs sham, p = 2.6e-6; vs water, p = 0.24).
d–o, Imaging of VTA-DA/CCK neurons. d, Fiber placement (left). Dynamics following water infusion (right).
e, Activity rose 36±7 s after Ensure reached the stomach. f, PC1 separates transient vs prolonged subtypes from k-means clustering. g, Population-weighted activity (left) and cumulative distributions (right) showing increased activity after Ensure infusion (vs sham, p = 1.7e-4; vs water, p = 0.038). h, Correlation analyses indicate distinct responses to water vs Ensure infusion. i, Dynamics during consumption of Ensure, water or sham.
j, Population-weighted activity (left) and cumulative distributions (right) confirm greater responses during Ensure bouts (vs sham, p = 2.0e-15; vs water, p = 0.0013). k, Binned activity during Ensure bouts. l, Correlation analyses indicate distinct responses to water vs Ensure bouts. m, Overlap of neurons responding to water and Ensure. n, Correlation analyses indicate distinct responses during IG vs natural consumption. o, Overlap of neurons responding during IG and natural consumption.
ns > 0.05; *P < 0.05; **P < 0.01; ***P < 0.001; ****P < 0.0001. See Extended Data Table 3.

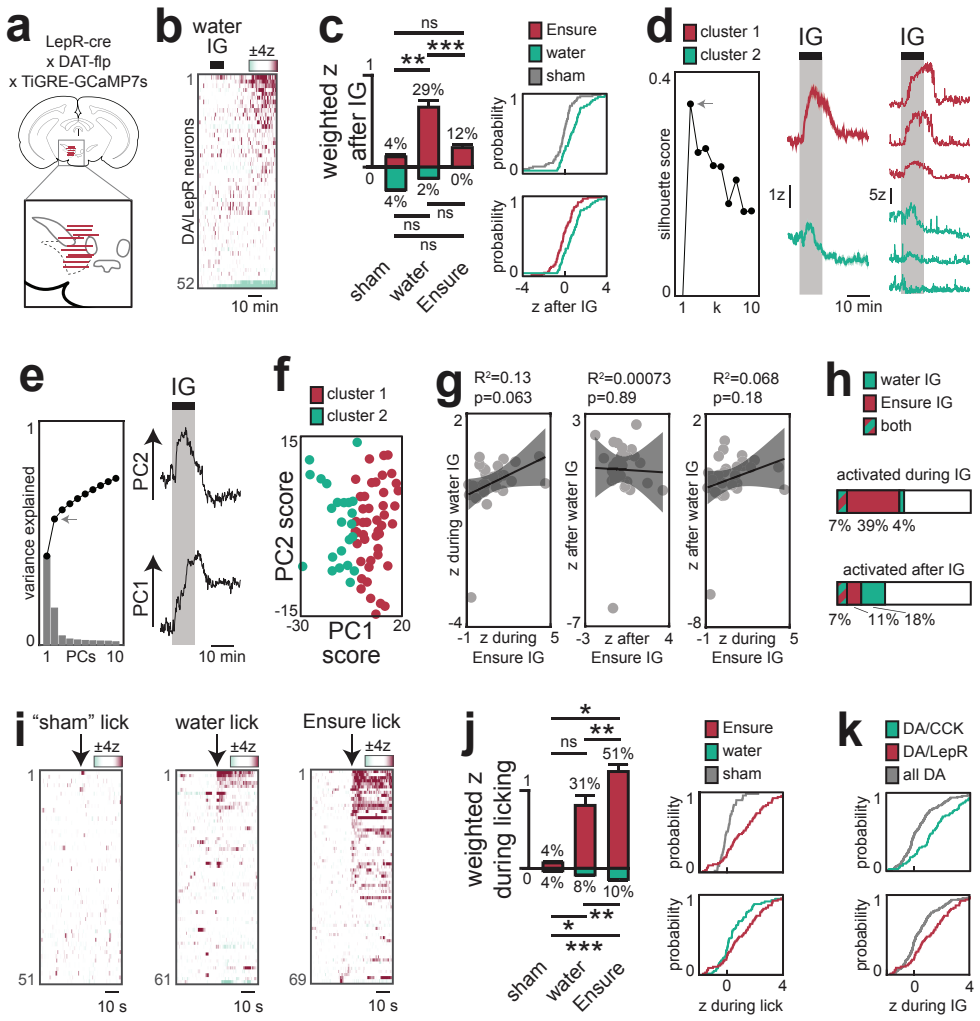

Extended Figure 8. DA/LepR subpopulation responses across different stages of ingestion.
a, Fiber placement for recording VTA-DA/LepR neurons.
b, Dynamics during water infusion.
c, Population-weighted activity (left) and cumulative distributions (right) show activation after water but not Ensure infusion (water vs sham, p = 6.9e-5; water vs Ensure, p = 0.0042; Ensure vs sham, p = 0.33).
d, K-means clustering reveals prolonged (purple) and transient (green) subpopulations, shown with mean and representative single-neuron activity.
e, Principal component analysis; the first two PCs explain 56% of variance and correspond to activity changes during and after infusion.
f, PC1 separates transient vs prolonged subtypes from k-means clustering.
g, Correlation analyses indicate distinct responses to water vs Ensure infusion.
h, Overlap of neurons responding to water and Ensure infusions.
i, Dynamics during consumption of Ensure, water or sham.
j, Population-weighted activity (left) and cumulative distributions (right) show increased activity during Ensure bouts (vs sham, 1.2e-6; vs water, p=0.045).
k, Cumulative distributions across subpopulations showed robust activation during Ensure consumption in both DA/CCK (p = 4.2e-11) and DA/LepR (p = 2.3e-12) groups.
ns > 0.05; *P < 0.05; **P < 0.01; ***P < 0.001; ****P < 0.0001. See Extended Data Table 3.

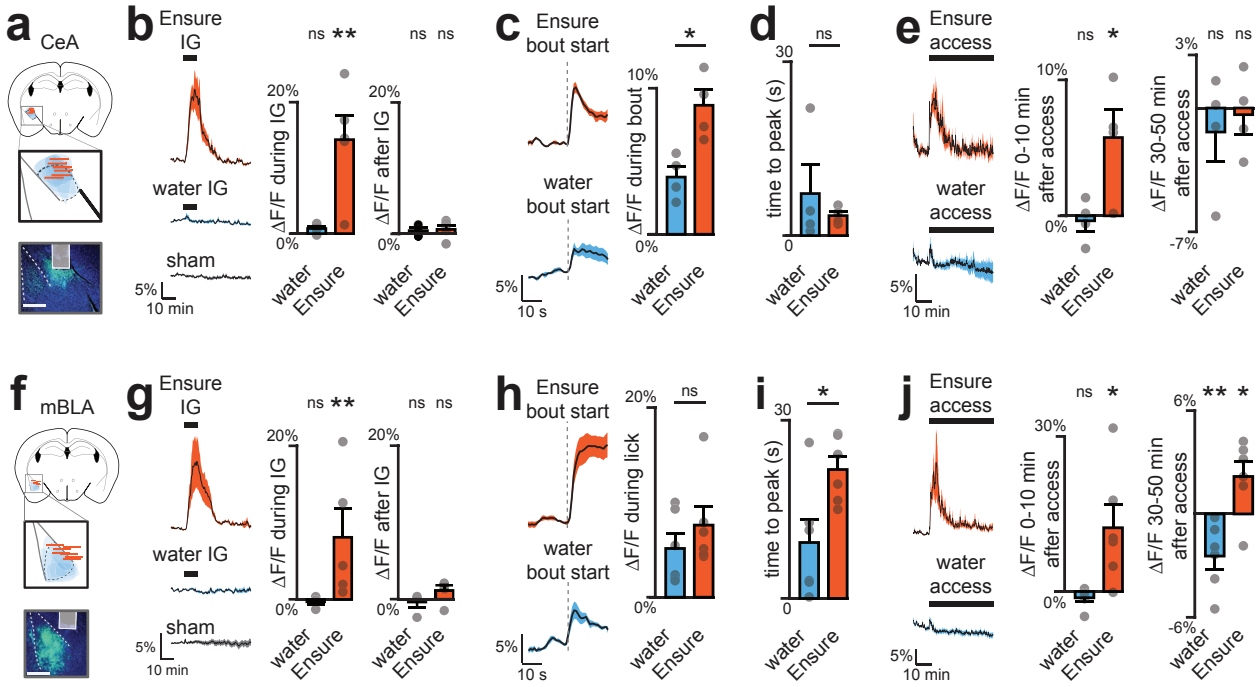

Extended Figure 9. DA release in neighboring mBLA and CeA during ingestion.
a–e, Fiber placement and viral spread for recording DA release onto CeA-VGAT neurons (a). DA increased during Ensure IG infusion compared to controls (b) and during the first lick bout (c), with no difference in peak timing across solutions (d). Mean activity remained elevated throughout consumption (e).
f–j, Fiber placement and viral spread for recording DA release onto mBLA-Vglut neurons (f). DA increased during Ensure IG infusion (g) and during the first lick bout (h), with peak release delayed for Ensure vs water (i). Mean activity remained elevated throughout consumption (j).
ns > 0.05; *P < 0.05; **P < 0.01; ***P < 0.001; ****P < 0.0001. See Extended Data Table 2.

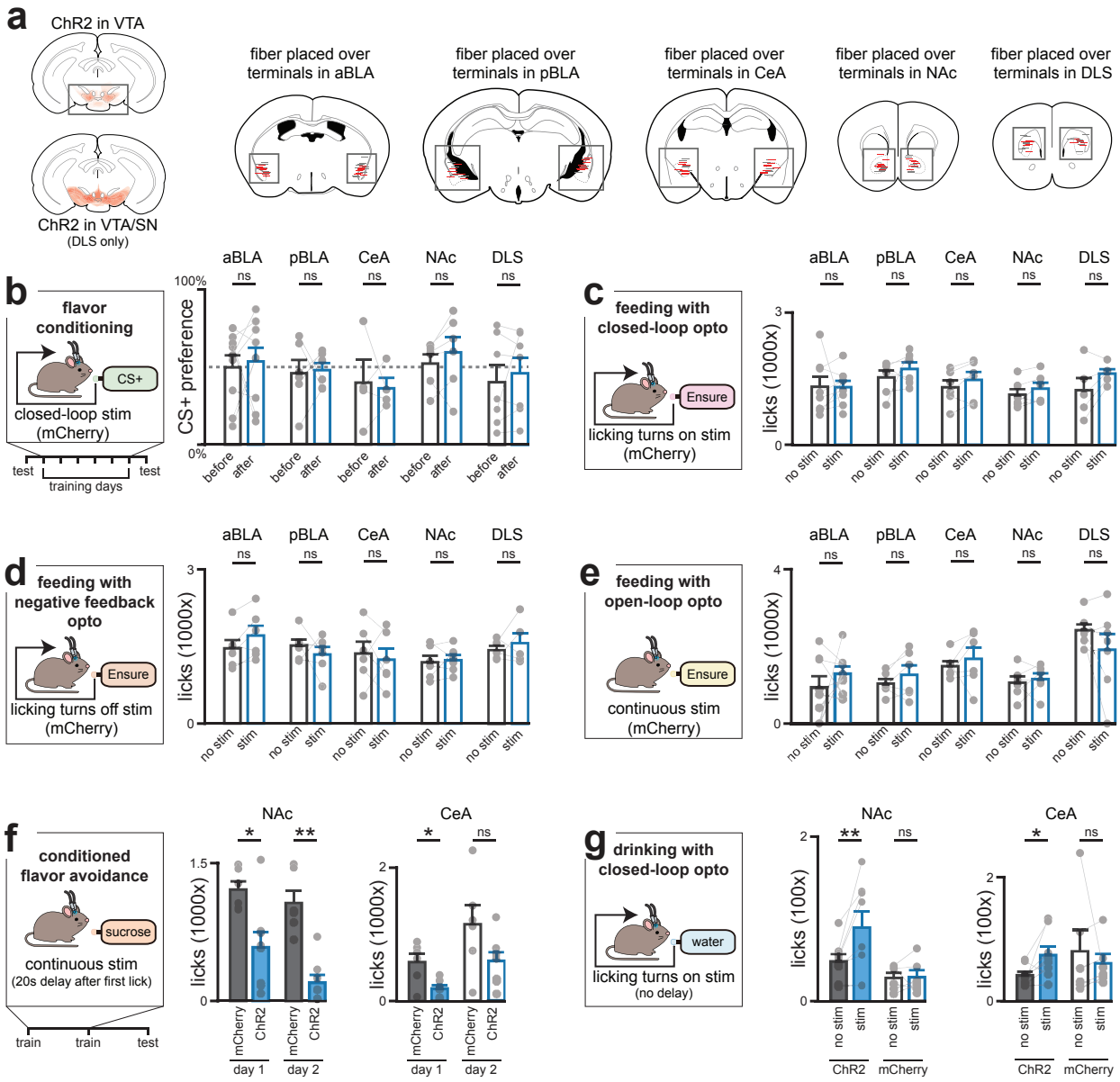

Extended Data Figure 10. Controls for dopamine projection experiments.
a, Viral expression of ChR2 in VTA-DA neurons (or all midbrain DA neurons for DLS terminal experiments) and fiber placement above projection targets (grey=mCherry, red=ChR2; see Fig. 4 for insets).
b, Flavor conditioning assay (mCherry controls; Fig. 4a).
c, Lick-activated stimulation (mCherry controls; Fig. 4d).
d, Lick-terminated stimulation (mCherry controls; Fig. 4e).
e, Continuous stimulation (mCherry controls; Fig. 4f).
f, Sucrose consumption during CFA training.
g, Lick-activated stimulation with water substituted for Ensure.
*P < 0.05; **P < 0.01; ***P < 0.001, after Benjamini–Hochberg correction (Extended Data Table 1).

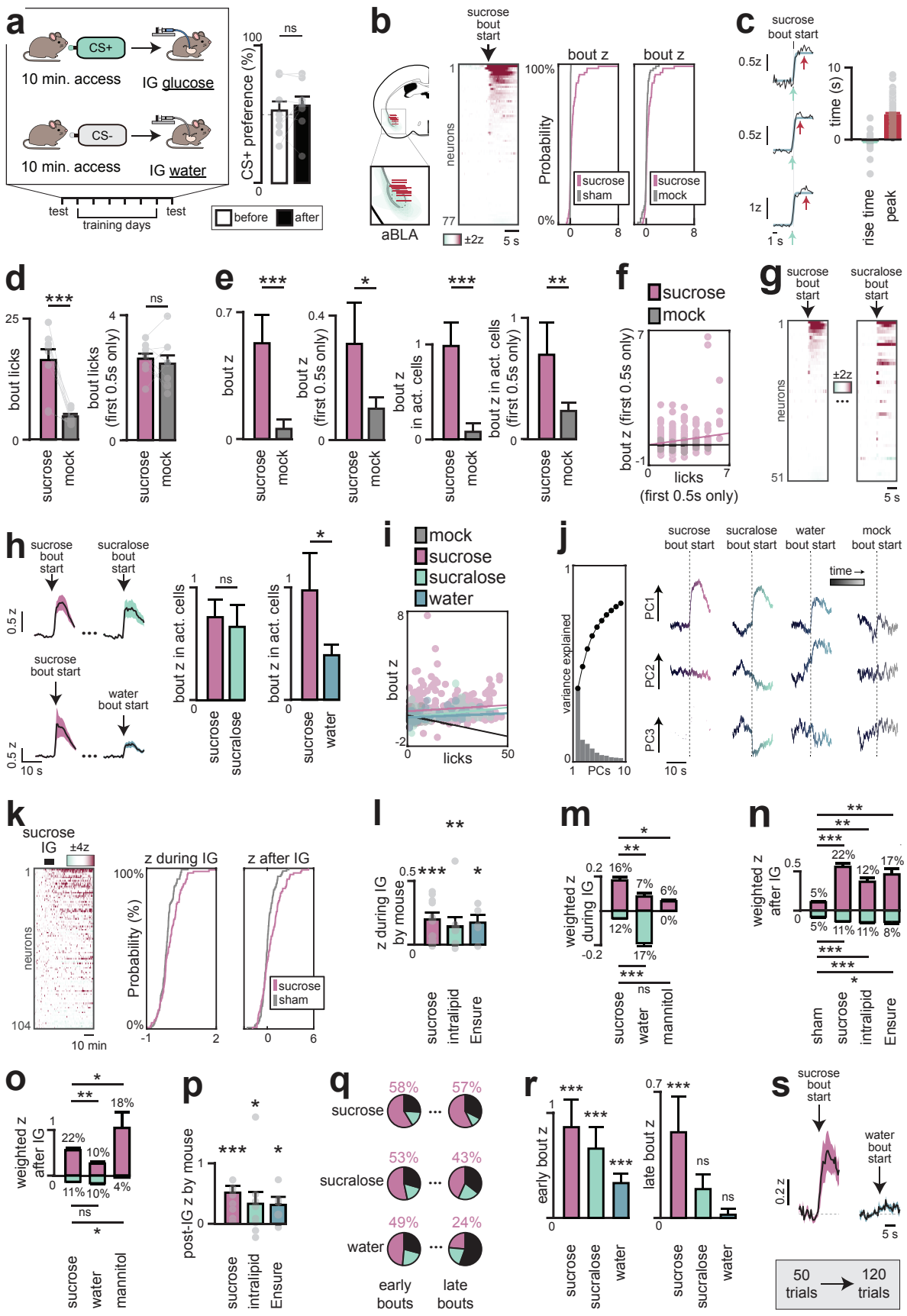
a
CS+
10 min. access
IG glucose
CS-
10 min. access
IG water
test
training days
test
CS+ preference (%)
100
0
ns
before
after
b
sucrose bout start
aBLA
neurons
1
77
±2z
5 s
bout z
bout z
100%
0%
Probability
sucrose
sham
sucrose
mock
0
8
0
8
c
sucrose bout start
0.5z
0.5z
1z
1 s
time (s)
10
0
rise time
peak
d
***
ns
bout licks
bout licks (first 0.5s only)
25
0
4
0
sucrose
mock
sucrose
mock
e
***
*
***
**
bout z
bout z (first 0.5s only)
bout z in act. cells
bout z in act. cells (first 0.5s only)
0.7
0
0.4
0
1
0
1
0
sucrose
mock
sucrose
mock
sucrose
mock
sucrose
mock
f
sucrose
mock
bout z (first 0.5s only)
7
-1
0
licks
(first 0.5s only)
7
g
sucrose bout start
sucralose bout start
neurons
1
51
±2z
5 s
h
sucrose bout start
sucralose bout start
0.5 z
sucrose bout start
water bout start
0.5 z
10 s
bout z in act. cells
1
0
ns
*
sucrose
sucralose
sucrose
water
i
mock
sucrose
sucralose
water
bout z
8
-2
0
licks
50
j
sucrose bout start
sucralose bout start
water bout start
mock bout start
time →
variance explained
1
0
1
PCs
10
PC1
PC2
PC3
10 s
k
sucrose
IG
±4z
neurons
1
104
10 min
z during IG
z after IG
100%
0%
Probability (%)
-1
2
0
6
sucrose
sham
l
**
z during IG by mouse
0.5
0
***
*
sucrose
intralipid
Ensure
m
*
**
weighted z during IG
0.2
-0.2
16%
7%
6%
12%
17%
0%
***
ns
sucrose
water
mannitol
n
**
**
***
weighted z after IG
0.5
0
22%
12%
17%
5%
5%
11%
11%
8%
***
***
*
sham
sucrose
intralipid
Ensure
o
*
**
weighted z after IG
1
0
22%
10%
18%
11%
10%
4%
ns
*
sucrose
water
mannitol
p
*
post-IG z by mouse
1
0
***
*
sucrose
intralipid
Ensure
q
58%
57%
sucrose
53%
43%
sucralose
49%
24%
water
early bouts
late bouts
r
***
***
***
early bout z
1
0
0.7
***
late bout z
ns
ns
0
sucrose
sucralose
water
sucrose
sucralose
water
s
sucrose bout start
water bout start
0.2 z
5 s
50 trials
120 trials

Extended Figure 11. aBLA neurons track sweet taste and nutrient information to drive learning.
a, Protocol for delayed flavor–nutrient conditioning. Mice received 10 min access to a flavored saccharin solution followed by IG infusion of water or glucose. Mice did not learn a preference if glucose infusion occurred only after licking ceased.
b, Fiber placement and viral spread for aBLA recordings. Averaged aBLA neuron dynamics during sucrose bouts (z-score) and distributions of activity compared to sham ($p = 6.7e-15$, KS test) or mock lick bouts ($p = 0.005$, KS test).
c, Peak (magenta) and 5% rise times (mint) with example cells (left) and summary plots (right).
d, Lick count across trials and during the first 0.5 s of bouts.
e, Activity of all cells (left) and sucrose-activated cells (right) across trials and during the first 0.5 s of bouts.
f, Correlation of activity and lick count during first 0.5 s of sucrose vs mock bouts (sucrose: $R^2 = 0.030$, $p = 0.0017$; mock: $R^2 = 0.00014$, $p = 0.95$).
g, Cross-registered neuron dynamics during sucrose (left) and sucralose (right) bouts.
h, Mean traces (left) and activity (right) of sucrose-activated neurons during sucrose vs sucralose and sucrose vs water bouts. Minor differences in sucrose activity reflect cross-registration.
i, Correlation of activity and lick count during mock, sucrose, sucralose, and water bouts (mock: $R^2 = 0.062$, $p = 0.21$; sucrose: $R^2 = 0.018$, $p = 0.016$; sucralose: $R^2 = 0.17$, $p = 1e-7$; water: $R^2 = 0.076$, $p = 0.0089$).
j, PCA of cross-registered neurons across sucrose, sucralose, and water sessions: scree plot (left) and first three PCs during each bout (right).
k, Single-neuron dynamics (left) and distribution of activity (right) during and after sucrose IG infusion (both: $p = 0.002$, KS test).
l, Population-weighted z-score activity during IG infusions, averaged by mouse.
m, Nutrient specific activation during IG infusion of sucrose, but not water or mannitol.
n, Activity after IG infusions.
o, Unlike early activation, post-IG activity is not nutrient-selective.
p, Population-weighted z-score activity after IG infusions, averaged by mouse.
q, Distribution of neurons activated (magenta), inhibited (mint), or unchanged (black) during early (bouts 2–6) vs late (last five) sucrose bouts. Percent activated given in magenta.
r, Late sucrose bouts (but not sucralose or water) activate these neurons.
s, Trial-based drinking sessions extended to 120 trials in a new cohort, which showed nutrient-specific bout responses.
ns $P > 0.05$; *$P < 0.05$; **$P < 0.01$; ***$P < 0.001$. See Extended Data Table 3.

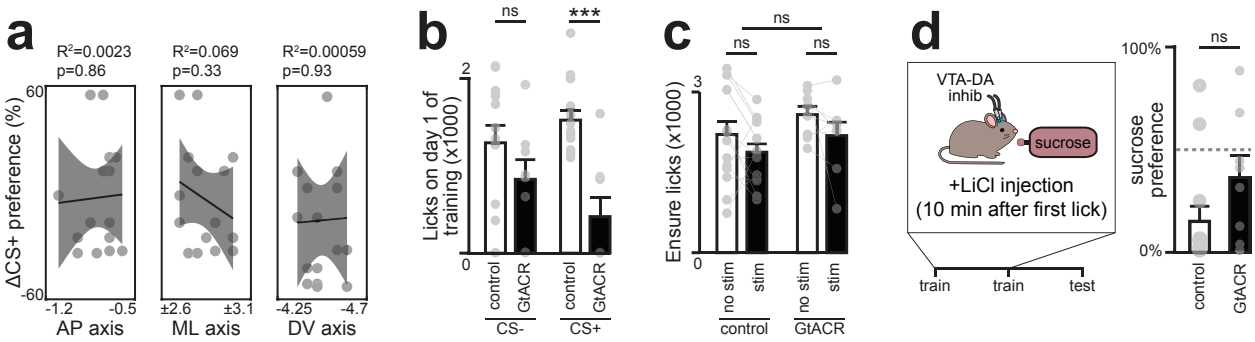

Extended Data Fig. 12. aBLA neurons are necessary for flavor-nutrient learning.
a, Preference differences were not explained by fiber localization across the three axes.
b, aBLA-D1R inhibition reduced CS+ intake on the first training day.
c, Continuous inhibition did not alter consumption of the familiar nutritive solution Ensure.
d, Conditioned flavor avoidance assay; inhibition during training did not block LiCl-induced aversion learning.
ns P > 0.05; *P < 0.05; **P < 0.01; ***P < 0.001. See Extended Data Table 1.

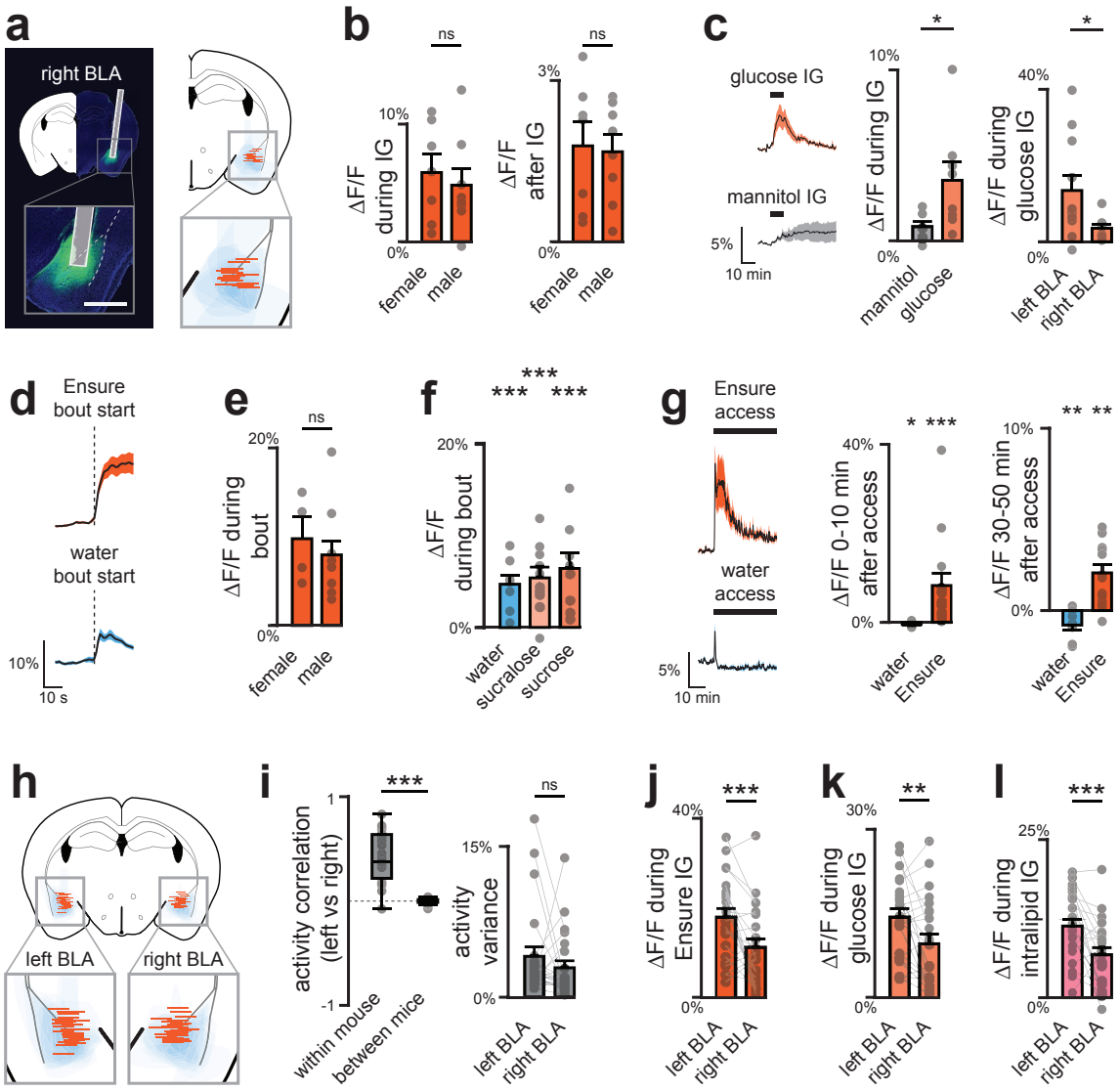

Extended Data Figure 13. Nutrient-triggered dopamine release in the right BLA.
a–g, Unilateral right BLA recordings.
a, Fiber placement and viral spread for GRAB-DA recording in right BLA (scale bar, 1 mm).
b, No sex differences in right BLA DA release during (left) or after (right) Ensure infusion.
c, Mean traces (left) and summary plots showing glucose responses in right BLA are nutrient-specific (middle) but smaller than in left BLA (right).
d, Mean trace showing DA release in right BLA during first bout of Ensure or water consumption.
e, No sex differences in right BLA DA release during first Ensure lick bout.
f, Summary plots of right BLA DA release during first lick bouts.
g, Traces (left) and summary plots (right) of right BLA DA release during Ensure or water consumption.
h–l, Bilateral BLA recordings.
h, Fiber placement and viral spread for simultaneous GRAB-DA recording in left and right BLA.
i, Spontaneous activity is coordinated (left) and comparable (right) across hemispheres.
j, Ensure responses are larger in left BLA.
k, Glucose responses are larger in left BLA.
l, Intralipid responses are larger in left BLA.
ns $P > 0.05$; *$P < 0.05$; **$P < 0.01$; ***$P < 0.001$. See Extended Data Table 2..

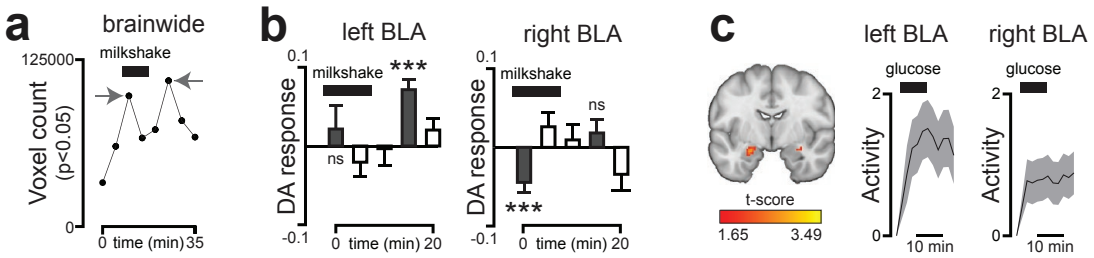

Extended Data Figure 14. Time course of lateralized activity and dopamine release in humans.
a, Number of brain-wide voxels (PET) showing increased dopamine release after milkshake consumption (normalized to water), with two peaks: an immediate oral signal (0–5 min after drinking onset) and a delayed post-ingestive signal (5–10 min after drinking offset).
b, Time course of dopamine release in left and right BLA. Significance shown for oral and post-ingestive time bins (grey bars).
c, Left and right BLA masks (left) and fMRI activity following glucose consumption (right). Activity was significant in left, but not right BLA.
ns $P > 0.05$; *$P < 0.05$; **$P < 0.01$; ***$P < 0.001$ (FWE-corrected). See Extended Data Table 4.

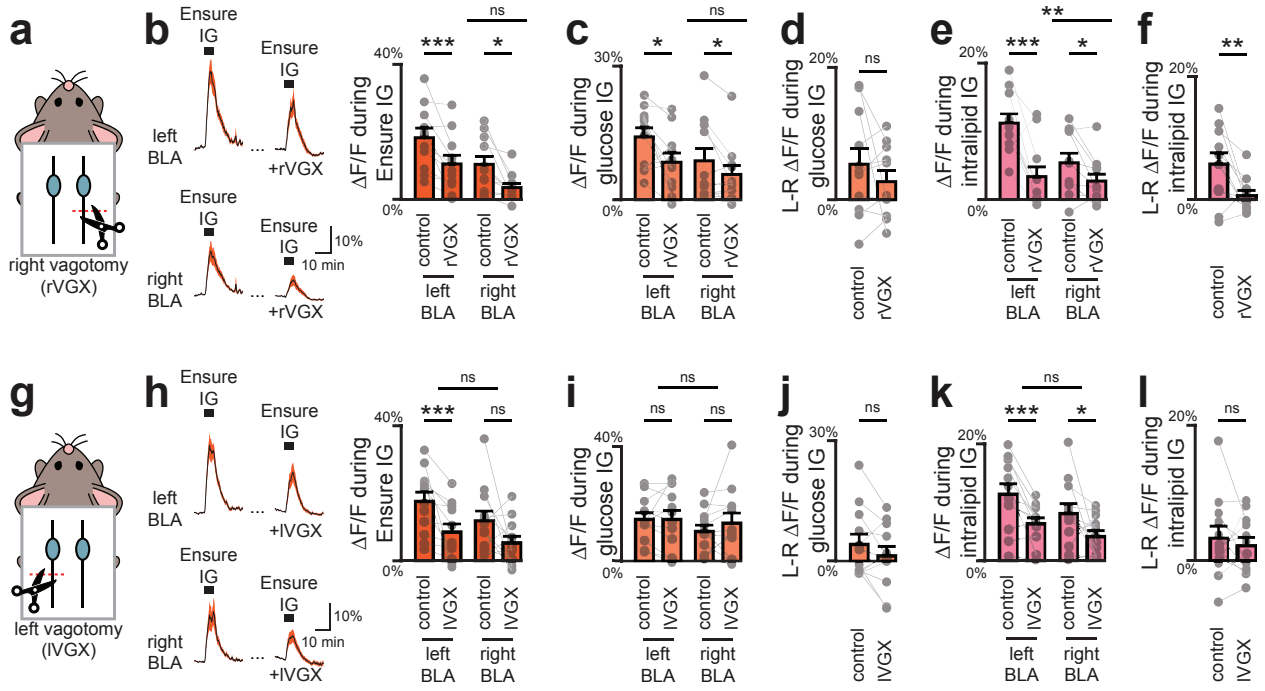

Extended Data Figure 15. Vagus nerve contributes to nutrient-triggered responses, but not lateralization of release.

a, Right vagotomy (rVGX).
b, Ensure responses in both hemispheres partially depend on right vagus.
c, Glucose responses in both hemispheres partially depend on right vagus.
d, Right vagotomy does not affect lateralized glucose responses.
e, Left BLA intralipid responses show greater sensitivity to right vagotomy.
f, Right vagotomy abolishes lateralized intralipid responses.
g, Left vagotomy (lVGX).
h, Ensure responses in both hemispheres partially depend on left vagus.
i, Left vagotomy does not affect glucose responses in either hemisphere.
j, Left vagotomy does not affect lateralized glucose responses.
k, Intralipid responses in both hemispheres partially depend on left vagus.
l, Left vagotomy does not affect lateralized intralipid responses.
ns $P > 0.05$; *$P < 0.05$; **$P < 0.01$; ***$P < 0.001$. See Extended Data Table 2..

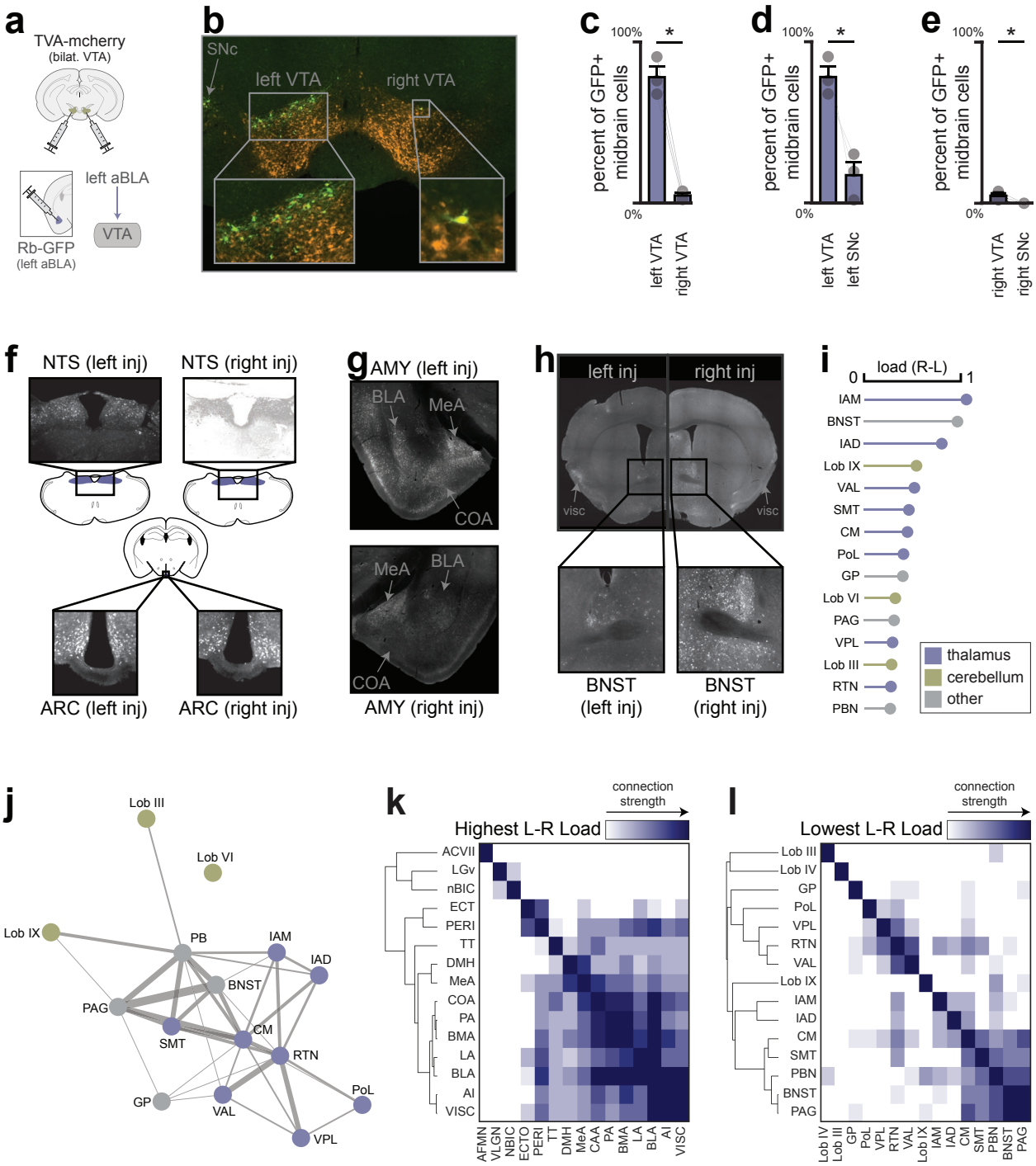
a
TVA-mcherry
(bilat. VTA)
left aBLA
VTA
Rb-GFP
(left aBLA)
b
SNc
left VTA
right VTA
c
100%
0%
*
percent of GFP+ midbrain cells
left VTA
right VTA
d
100%
0%
*
percent of GFP+ midbrain cells
left VTA
left SNc
e
100%
0%
*
percent of GFP+ midbrain cells
right VTA
right SNc
f
NTS (left inj)
NTS (right inj)
ARC (left inj)
ARC (right inj)
g
AMY (left inj)
BLA
MeA
COA
MeA
BLA
COA
AMY (right inj)
h
left inj
right inj
visc
visc
BNST
(left inj)
BNST
(right inj)
i
load (R-L)
0
1
IAM
BNST
IAD
Lob IX
VAL
SMT
CM
PoL
GP
Lob VI
PAG
VPL
Lob III
RTN
PBN
thalamus
cerebellum
other
j
Lob III
Lob VI
Lob IX
PB
IAM
IAD
BNST
PAG
SMT
CM
RTN
PoL
GP
VAL
VPL
k
connection strength
Highest L-R Load
ACVII
LGv
nBIC
ECT
PERI
TT
DMH
MeA
COA
PA
BMA
LA
BLA
AI
VISC
AFMN
VLGN
NBIC
ECTO
PERI
TT
DMH
MeA
CAA
PA
BMA
LA
BLA
AI
VISC
l
connection strength
Lowest L-R Load
Lob III
Lob IV
GP
PoL
VPL
RTN
VAL
Lob IX
IAM
IAD
CM
SMT
PBN
BNST
PAG
Lob IV
Lob III
GP
PoL
VPL
RTN
VAL
Lob IX
IAM
IAD
CM
SMT
PBN
BNST
PAG

Extended Data Figure 16. Networks underlying dopamine lateralization.

a, Rabies tracing of DAT+ midbrain neurons projecting to left aBLA. Cre-dependent TVA was expressed in VTA/SNc, followed 3 weeks later by injection of CVS-N2c-dG-mGFP in left aBLA.

b, Labelled midbrain cells 1 week after rabies injection, showing strong ipsilateral bias. Insets show a single contralateral VTA cell; some labeling in ipsilateral SNc.

c–e, Quantification of labeled cells: 78 ± 7% ipsilateral VTA, 17 ± 8% ipsilateral SNc, 5 ± 2% contralateral VTA, and none in contralateral SNc.

f, Cells labelled four days after PRV-Introvert-GFP injection into left BLA and right BLA of DAT-cre mice. No substantial differences observed in the
nucleus of the solitary tract (NTS) or arcuate nucleus (ARC), where nutrient signals enter the brain.

g, Greater labelling of several amygdalar regions after left-side injection.

h, Greater labelling of BNST following right vs left injection (arrows indicate VISC showing greater labelling after left injection).

i, Top fifteen regions that demonstrated strongest labelling after injection into right vs left BLA.

j, Force-directed graph showing connectivity between areas in (e).

k–l, Connectivity matrixes and hierarchical clustering of areas with greatest labelling after injection into left vs right BLA (f) or right vs left BLA (g).

Abbreviations (used here and Fig. 6): ACVII, accessory facial motor nucleus; AI, agranular insula; ARC, arcuate nucleus; BLA, basolateral amygdala; BMA, basomedial amygdala; BNST, bed nuclei of the stria terminalis; CM, central medial nucleus of the thalamus; COA, cortical amygdala area; DECLIVE, lobule VI (declive); DMH, dorsomedial nucleus of the hypothalamus; ECT, ectorhinal area; GP, globus pallidus; IAM, interanteromedial nucleus of the thalamus; IAD, interanterodorsal nucleus of the thalamus; LA, lateral amygdala; LGv, ventral lateral geniculate; Lob III, lobule III; Lob IX, uvula; MeA, medial amygdala; nBIC, nucleus of the brachium of the inferior colliculus; NTS, nucleus of the solitary tract; PA, posterior amygdala; PAG, periaqueductal gray; PBN, parabrachial nucleus; PERI, perirhinal area; PoL, posterior limiting nucleus of the thalamus; RTN, reticular nucleus of the thalamus; SMT, submedial nucleus of the thalamus; TT, taenia tecta; VAL, ventral anterior-lateral complex of the thalamus; VISC, visceral area; VPL, ventral posterolateral nucleus of the thalamus.